Tectonics

RESEARCH ARTICLE
10.1029/2023TC007806

Oblique Collision of the Bahamas Platform at the Northern Boundary of the Caribbean Plate Recorded by the Late Cenozoic Coastal Terraces of SE Cuba

Christine Authemayou[1], Arelis Nuñez[2], Kevin Pedoja[3], Leandro Peñalver[2], Denovan Chauveau[4], Pedro Dunán-Avila[1], Denyse Martin-Izquierdo[2], Gino de Gelder[5], Laurent Husson[6], Enrique Castellanos Abella[7], Pedro de Jesús Benítez Frómeta[2], and Anne-Morwenn Pastier[8]

[1]Geo-Ocean UMR 6538, CNRS, Ifremer, Université de Bretagne Occidentale, Plouzané, France, [2]Institute of Geology and Paleontology, La Habana, Cuba, [3]Normandie Univ, UNICAEN, UNIROUEN, Caen, France, [4]Dipartimento di Scienze Ambientali, Informatica e Statistica Università Ca'Foscari, Venezia, Italy, [5]Research Group of Paleoclimate and Paleoenvironment, Research Centre for Climate and Atmosphere, Research Organization of Earth Sciences and Maritime, National Research and Innovation Agency, Bandung, Republic of Indonesia, [6]ISTerre, CNRS, UMR 5275, Université de Grenoble Alpes, Grenoble, France, [7]Director de geologia, Ministry of Energy and Mines, La Habana, Cuba, [8]Helmholtz Centre Potsdam, German Research Centre for Geosciences (GFZ), Potsdam, Germany

Abstract The southeastern tip of Cuba Island is limited to the south by the N-Caribbean boundary. By revisiting the impressive sequences of coastal terraces of this region, we decipher the Quaternary deformation pattern of this plate boundary. We present a detailed mapping of coastal terraces uplifted over a hundred kilometers of coastline, and U/Th dating. At Punta de Maisí, the deformation pattern shows (a) a faster uplift close to the transform boundary and (b) a northward propagation of folding produced by the convergence of the Bahamas platform toward the Caribbean plate. Along the southern coast of Punta de Maisí, the sequence displays 29 coastal terraces up to 520 m in elevation and a upper Pleistocene uplift rate of 0.23 ± 0.07 mm yr^{-1}. We interpret this deformation as resulting from an offshore north-dipping reverse fault near the coast. This uplift rate corresponds to 3% to 1.6% of the short-term horizontal slip rate of Septentrional Oriente Fault Zone (10 ± 0.1 mm yr^{-1}). Along the northern coast of Punta de Maisí, the sequence displays height coastal terraces up to 220 m in elevation and the uplift rates amount to 0.1 ± 0.05 mm yr^{-1} and likely result from the reverse faulting and folding associated with the offshore North Hispaniola Fault Zone. Uplift rates quickly decrease to the West, in agreement with the westward decrease in the activity of the North Hispaniola Fault Zone due to the docking of the Bahamas Platform against Cuba, while the platform more gently underthrusts Cuba to the East.

Key Points:

- In SE of Cuba, the maximum uplift rate is 0.23 mm/yr and there is a maximum of 29 coastal terraces in a 520 m high sequence
- The upper and middle coastal terraces of the sequences are tilted to the north and show northward folding
- The uplift gradient expresses the docking of the Bahamas Platform against Cuba to the W, while the platform underthrusts Cuba to the E

Correspondence to:
C. Authemayou,
christine.authemayou@univ-brest.fr

Citation:
Authemayou, C., Nuñez, A., Pedoja, K., Peñalver, L., Chauveau, D., Dunán-Avila, P., et al. (2023). Oblique collision of the Bahamas platform at the northern boundary of the Caribbean plate recorded by the Late Cenozoic coastal terraces of SE Cuba. *Tectonics*, *42*, e2023TC007806. https://doi.org/10.1029/2023TC007806

Received 16 FEB 2023
Accepted 14 JUL 2023

Author Contributions:
Conceptualization: Christine Authemayou, Leandro Peñalver
Formal analysis: Christine Authemayou, Pedro Dunán-Avila
Funding acquisition: Christine Authemayou
Investigation: Christine Authemayou, Arelis Nuñez, Kevin Pedoja, Leandro Peñalver, Denovan Chauveau, Denyse Martin-Izquierdo, Gino de Gelder, Pedro de Jesús Benítez Frómeta
Methodology: Arelis Nuñez, Kevin Pedoja
Project Administration: Christine Authemayou, Kevin Pedoja, Leandro Peñalver, Enrique Castellanos Abella
Software: Christine Authemayou, Arelis Nuñez, Anne-Morwenn Pastier
Supervision: Christine Authemayou

1. Introduction

The transform boundary between the Caribbean and the North American plates extends from Guatemala (W), to Puerto Rico Island (E) where it connects to the Caribbean subduction zone (Figure 1). In its central part, this plate boundary consists of two transform fault zones, the Septentrional Oriente Fault Zone (SOFZ, to the N) and Enriquillo-Plantain Garden Fault Zone (EPGFZ, to the S). The faults frame the Gonave block. Along this EW-trending plate boundary, the North American plate moves westward at a rate of 18–20 ± 3 mm yr^{-1} relative to the Caribbean plate producing highly oblique convergence (20°–10° of obliquity) (Calais et al., 2016; DeMets et al., 2000; Mann et al., 2002) (Figure 1). The SOFZ separates the Cuban archipelago to the north from the Hispaniola archipelago to the south (Figure 1). These islands belonged to the Cretaceous Caribbean arc before being separated during the Tertiary by the southward jump of the plate boundary from the northern Cuban margin to its present location in the southern Cuban margin (Cruz-Orosa et al., 2012; Leroy et al., 2000; Rojas-Agramonte et al., 2006). This change of plate boundary location resulted from the oblique collision of the Cretaceous Caribbean arc with the southern margin of the North American plate, which includes the 2- to 5-km thick buoyant Bahamas platform (Calais et al., 2002, 2016; Dolan and Mann, 1998; Mann et al., 2002, 2004; Rodriguez-Zurrunero et al., 2020; Uchupi et al., 1971; Van Benthem et al., 2014) (Figure 1b). Since the Miocene, the oblique collision is accommodated north of the SOFZ and the Hispaniola archipelago, by the underthrusting of the Bahamas platform along the offshore North Hispaniola Fault Zone (Oliveira de Sá et al., 2021; Pubellier et al., 2000; Rodríguez-Zurrunero et al., 2020). East of the Bahamas platform, the North Hispaniola Fault Zone continues along the Puerto Rico trench that accommodates the North American subducting slab (DeMets

Validation: Christine Authemayou, Arelis Nuñez, Kevin Pedoja, Leandro Peñalver, Denovan Chauveau, Denyse Martin-Izquierdo
Visualization: Kevin Pedoja, Leandro Peñalver, Denovan Chauveau, Pedro Dunán-Avila, Gino de Gelder, Laurent Husson, Enrique Castellanos Abella, Pedro de Jesús Benítez Frómeta, Anne-Morwenn Pastier
Writing – original draft: Christine Authemayou
Writing – review & editing: Arelis Nuñez, Kevin Pedoja, Leandro Peñalver, Denovan Chauveau, Pedro Dunán-Avila, Gino de Gelder, Laurent Husson

et al., 2000; Rodriguez-Zurrunero et al., 2020; Ten Brink, 2005). The western termination of the North Hispaniola Fault Zone has not been precisely mapped, but evidence of offshore deformation associated with its activity as far west as the town of Moa (Cuba), suggests that the fault is present at least in the northern part of eastern Cuba (Dentzer et al., 2021; Rodríguez-Zurrunero et al., 2020). South of the SOFZ, the oblique collision lead to the uplift of the Haitian and Dominican coasts recorded by sequences of coral and marine terraces (Dodge et al., 1983; Dumas et al., 2006; Escuder-Viruete et al., 2020; Hearty et al., 2007; Mann et al., 1995). North of the transform plate boundary, uplifted sequences of coastal (i.e., marine and coral reef) terraces all along the Cuban coast suggest that the Bahamas oblique collision is accommodated over a much larger spatial area than the Hispaniola archipelago (Peñalver et al., 2021) (Figure 1). Although studied for more than a century, few marine terraces of Cuban sites have been dated (see synthesis in Peñalver et al., 2021). To our knowledge, only De Waele et al. (2018), Muhs et al. (2017), Schielein et al. (2020), and Toscano et al. (1999) published Last Interglacial ages derived from ESR and U-Th dating in the Matanzas in northern Cuba zone and Guantánamo in southern Cuba zone.

Here, we investigate the Cuban coastal terrace sequences located in the southeastern tip of Cuba, which are after the ones formed in Haiti among the most elevated (∼500 m) in the Caribbean realm. This zone lies at the transition between the transform plate boundary to the South and the poorly constrained western tip of the North Hispaniola Fault Zone to the North. The analysis of these coastal terraces allows for documenting the temporal and spatial distribution of Late Cenozoic deformation during the oblique collision of the Bahamas platform. We mapped the distribution of the sequences of coastal terraces over a 120-km long coastal stretch, on high-resolution Pleiades Digital Elevation Model (DEM) combined with differential GPS data. We completed the analysis by determining the regional altitudinal variations of the upper coastal terraces with projected topographic swath profiles. We U/Th dated the lowermost marine terraces and evaluated uplift rates. Finally, we discuss the results in the framework of the Bahamas platform oblique collision, the westward propagation of the North Hispaniola Fault Zone and the role of the SOFZ in the accommodation of the oblique convergence south of Cuba.

2. Settings

2.1. Geological Setting

The Cuba Island archipelago is located on the North American plate at its boundary with the Caribbean plate (Corbeau et al., 2017; Núñez et al., 2019) (Figure 1). The main island of Cuba archipelago is 1,200 km -long and up to 210 km -wide. It consists of a NW-SE-trending fold-and-thrust belt disrupted by ENE-WSW faults and Tertiary basins. The belt includes Early Cretaceous to Campanian arc rocks, ocean crust, sub-oceanic mantle, metamorphosed continental crust and syn-and post-orogenic deposits. This orogenic belt resulted from the Late Cretaceous to Paleogene accretion/collision of the Greater Antilles Island arc with the Bahamas and Yucatan platforms of the North American continental margin (Burke, 1988; Cruz-Orosa et al., 2012; Iturralde-Vinent, 1994; Pindell & Dewey, 1982; Saura et al., 2008). During Paleocene (56 Ma), the buoyant Bahamas Platform entered the Greater Caribbean subduction zone at its eastern tip and collided diachronically with the volcanic arc from west to east. Following this collision, the North American plate motion direction changed from southwestwards to westwards (Boschman et al., 2014). During this time, left-lateral strike-slip faults in Cuba (i.e., Pinar, Trocha, and Cauto-Nipe-Guacanayabo faults) progressively relocated the plate boundary from the north to the south of Cuba (Figure 1b), fragmenting the fold-and-thrust belt and bounding Neogene post-orogenic basins (Cruz-Orosa et al., 2012; Gordon et al., 1997; Iturralde-Vinent & MacPhee, 1999; Leroy et al., 2000; Rojas-Agramonte et al., 2006; Rosencrantz, 1990). The northern boundary of the Caribbean plate shifted to its current position along the Cayman trough and the SOFZ during the Oligocene (Calais & De Lépinay, 1995; Leroy et al., 2000; Mann, 1997) and connect the Septentrional fault as SOFZ in the Pliocene (Oliveira de Sá et al., 2021). Along the northern Cuban margin, the oblique collision led to the suture of the subduction zone (Gordon et al., 1997; Pindell et al., 2005). This structure is currently reactivated southeastward of Cuba as the western extension of the North Hispaniola Fault Zone (Oliveira de Sá et al., 2021). Since the Late Cenozoic, the collision progressively uplifts the Cuba and Hispaniola islands (Calais et al., 1992; Escuder-Viruete and Pérez, 2020; Mann et al., 1991; Pubellier et al., 2000; Symithe et al., 2015; Wessels, 2019). The uplift was recorded by the formation and preservation of sequences of coastal terraces alongshore Cuba and Hispaniola (e.g., de Neira et al., 2015; Escuder-Viruete et al., 2020; Mann et al., 1995; Peñalver et al., 2021) (Figure 1).

The Punta de Maisí, at the southern tip of Cuba (Figure 2), belongs to the Septentrional block bounded by the North Hispaniola Fault Zone (north) and by the SOFZ (south) (Figure 1b). The Septentrional block defines a

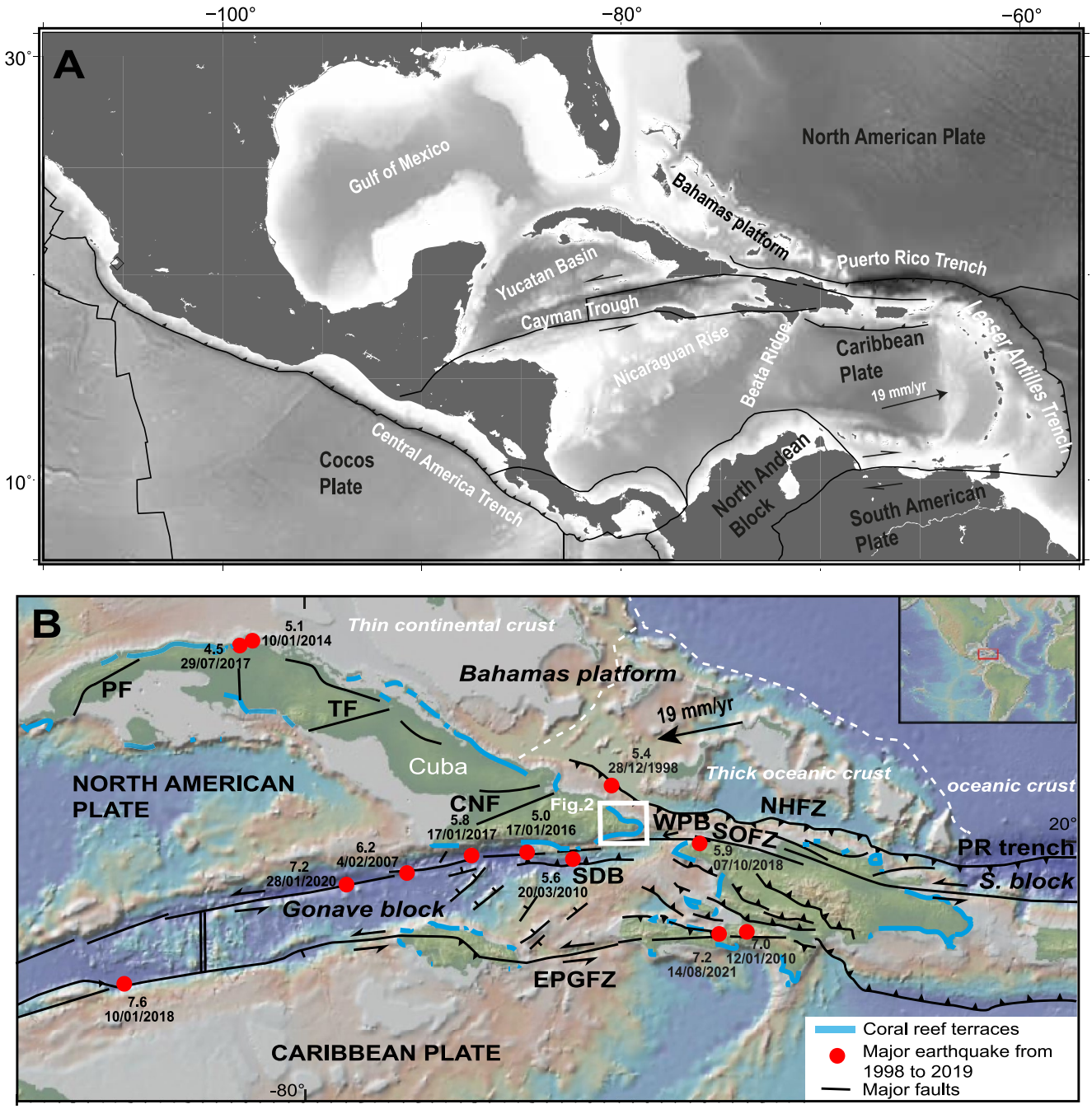

Figure 1. Geodynamics of the Cuban and Hispaniola archipelagos. (a) Geodynamic framework. (b) Tectonic pattern, sequences of coastal terraces and location of major earthquakes. Bahamas platform with crust nature contoured in white dashed line (Ladd & Sheridan, 1987; Román et al., 2021; Uchupi et al., 1971). PF: Pinar fault, TF: la Trocha Fault, CNF: Caute Nipe Fault, NHFZ: North Hispaniola Fault Zone, SOFZ: Septentrional Oriente Fault Zone; EPGFZ: Enriquillo-Plantain-Garden Fault Zone; S. block: Septentrional block; SDB: Santiago Deformed Belt, PR trench: Puerto Rico trench.

forearc sliver with a narrow accretionary prism in the offshore sector of northern Hispaniola and Puerto Rico (Dillon et al., 1993; Dolan & Mann, 1998; Escuder-Viruete et al., 2020; Rodriguez-Zurrunero et al., 2019). To the east of the Punta de Maisí, geophysical data shows a longitudinal basin (Windward Passage Basin) and a high topographic plateau (Windward Passage Sill), with Tertiary to Quaternary deformed sediments (Oliveira de Sá et al., 2021) (Figure 1). Several tectonic events were recorded in the Windward Passage Sill and Basin related to the ongoing oblique collision between the Caribbean plate and the Bahamas platform (Escuder-Viruete et al., 2020; Oliveira de Sá et al., 2021). Transpressional Pliocene deformation produced a pop-up structure on both sides of

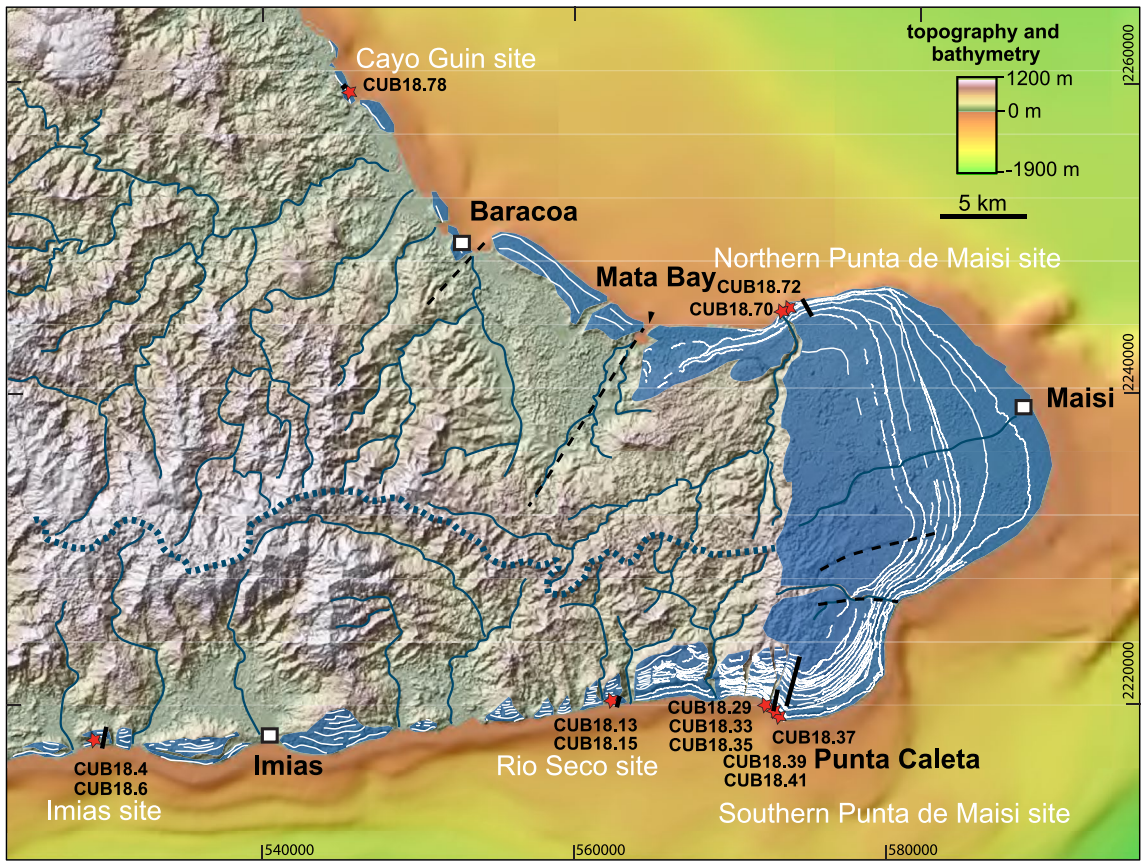

Figure 2. Sequences of coastal terraces of SE Cuba. The sequences are mapped in blue and their inner edges in white lines. Red stars are sample locations with sample names. Black lines are topographic profile locations and dashed black lines are normal faults. Blue lines and dashed blue line are the rivers and the main drainage divide, respectively.

the Windward Passage Sill and a flower structure in the Windward Passage Basin (Calais et al., 1992, 2016; Leroy et al., 2015; Oliveira de Sá et al., 2021).

2.2. Coastal Terraces of the Southeastern Tip of Cuba

The coastal terraces of the southeastern tip of Cuba are formed by different reefal limestone units constructed and eroded during successive Quaternary sea-level oscillations as observed at different sites on the world's coasts (e.g., Chauveau et al., 2021; Hearty et al., 2007; Major et al., 2013; Peñalver et al., 2021). Their abundance and their preservation attracted attention since the end of the nineteenth century (Agassiz, 1894; Busto, 1975; Crosby, 1883; del Corral, 1944; Diaz et al., 1991, 2011; Furrazola-Bermūdez, 1964; Hill, 1895; Horsfield, 1975; Iturralde-Vinent, 2003; Núñez Jiménez, 1973; Peñalver et al., 2003, 2021; Vaughan & Spencer, 1902). The most ubiquitous is the low-elevation terrace (formed by the Jaimanitas formation) of Last Interglacial age (Cabrera & Peñalver, 2001; Iturralde-Vinent, 2009; Peñalver et al., 2003, 2021; Portell et al., 2008, 2009; Rojas-Agramonte et al., 2005; Toscano et al., 1999). The highest coastal terraces in Punta de Maisi were formed by marine erosion on a Mio-Pliocene carbonate substratum (Busto, 1975). Paleomagnetic dating on these upper terraces reveals ages up to 4 Ma (Peñalver et al., 2003). In Baracoa (Figure 2), to the northwest of the studied zone, three levels are well marked (2 m, 27 m, 75 m in altitude), followed by a fourth, higher level at 150–180 m that is less well preserved (del Corral, 1944). A fifth level flattens the highest relief in the region, the Yunque massif at 557 m (Peñalver et al., 2021). To the East, at Punta de Maisí, del Corral (1944) presented height marine terraces on the Maisí coastline at heights of 2–15, 50–100, 130–180, 200–260, 300–380, 410–450, and 520 m. Núñez Jiménez (1973) published a map showing 15 coastal terraces up to 500 m in the Maisí region. Busto (1975) maps up to 19 terraces in the same area. Peñalver et al. (2021) determined from 7 to 25 levels varying toward the south. According to the northward inclination of the upper marine terraces and the greatest number of terraces in the southern part of the studied zone, Horsfield (1975) suggested the highest uplift rate in Cuba south of Punta de Maisí.

3. Materials and Methods

3.1. Mapping of Uplifted Coastal Terraces

The staircase morphology of a sequence of coral reef and marine terraces marks the interplay between primary coastal morphology (which can be composite, with several superimposed reefal limestone units), marine erosion which flattens and widens the inner part by cliff retreat during emergence and reduces the distal part by cliff retreat during and just after emersion (e.g., Chauveau et al., 2021; Husson et al., 2018; Pastier et al., 2019; Pedoja et al., 2018). The inner edge and associated shoreline angle of marine terraces correspond to the base of these ancient sea cliffs and can be recognized by an abrupt change in slope (Lajoie, 1986; Pedoja et al., 2011, 2014). Sometimes a tidal notch may form that could be used by a karst formed in the mixing zone between fresh and brackish water (Mylroie & Carew, 1990; D'Angeli et al., 2015).

We mapped the shoreline angle of coastal terraces using dGPS topographic profiles and 5 and 2 m high-resolution DEM of produced from ALOS (NTTDATA, RESTEC Included © JAXA) and Pleiades CNES stereoscopic satellite images, respectively. With the help of the different data sets (hillshades, slope maps, satellite ortho-images, and field data), we contoured the inner edges of each preserved surfaces corresponding to the fossil cliffs from 0 to 520 m above the current sea level with the ESRI's ArcGIS 10 software. The lateral correlation of coastal terraces across valleys, is based on the continuity of elevations, planform width, and equivalent position in the terrace sequence. We attribute a number to each terrace between T0 and T29 (T0 being the active terrace and T29 the uppermost one). We acquired topographic profiles at the five sites, using a real kinematic differential global positioning system (RTK dGPS) (Figure 2). Our profiles were carried out perpendicular to the main inner edges of the successive coastal terraces starting from the mean sea level. The roughness of the successive coastal terraces and continental slope deposits at the base of the paleo-cliffs of the inner edge are the main source of error in elevation, far beyond instrumental errors. Consequently, we assigned an elevation uncertainty of 1 m to all field measurements.

We also selected 6 major most continuous terraces named TA to TF from sea level upwards. We used hundreds of parallel topographic swaths from DEM of narrow width staked together perpendicular to their strike (Armijo et al., 2015; de Gelder et al., 2022). The elevation of their inner edges was mapped onto these stacked swath profiles, in order to measure their cumulated deformation. Distortion of the terraces would depend on the viewing angle with respect to the dip of the terraces; minimizing the distortion of the terrace sequence indicates the tilting direction. Folded terraces display their maximal flexure when profiles are perpendicular to the fold axis.

3.2. Sampling Strategy and U/Th Dating

We focused on five sites around the southeastern peninsula of Cuba (Figure 2). We extracted samples of corals for U/Th dating, by drilling coral colonies in growth positions from the surface of the coral reef terrace to date the constructional phases, as well as on reworked corals in the sinter cover at the fossil notch to date the morphological structure, likely close to the date of a sea level stand. Low terraces were preferentially sampled to minimize the risk to sample recrystallized coral (from aragonite to calcite) that would prevent reliable dating. We took 89 samples out of which we selected 13 that were not recrystallized.

The samples were mechanically cleaned with a micro-drill and then crushed, rinsed in MilliQ water and leached in 0.1 N bi-distilled HCL for 15–20 min in an ultrasonic bath. The cleaned samples were then crushed into powder and analyzed using a XRD Brucker D8 at the LCG (Laboratoire d'étude des "Cycles Géochimiques et Ressources", IFREMER) in Brest (France) to quantify the relative quantities of calcite and aragonite. We proceeded with U-Th dating on aragonitic samples (aragonite > 90%).Subsequently, the powders were dissolved in 7N HNO_3 and a mixed ^{229}Th-^{233}U-^{236}U spike was added to the solution and allowed to equilibrate. A detailed description of the calibration of the spike is given by Gibert et al. (2016). After drying down the solutions, the residues were treated with a mixture of concentrated HNO_3, HCl, and H_2O_2 to remove the remaining organic components. Then, the solutions were dried again and dissolved in 6N HCl. The fractions of U and Th were then separated from the $CaCO_3$ matrix as described by Yang et al. (2015). For mass spectrometric analysis, the U and Th fractions were dissolved in 2 mL of 0.8 N HNO_3. The U and Th isotopic compositions were analyzed on a Multi-Collector Inductively Coupled Plasma source Mass Spectrometer (MC-ICPMS) Thermo ScientificTM NeptunePlus fitted with a jet pump interface and a dissolving introduction system (aridus II). For mass fractionation correction, we used an exponential law (normalized to natural $^{238}U/^{235}U$ isotopic ratio) and

standard/sample bracketing. More details on the analytical procedure (chemistry and MC-ICPMS analysis) can be found in Pons-Branchu et al. (2014). After corrections for peak tailing, hydrate interference and chemical blanks, $^{230}Th/^{234}U$ ages were calculated from measured atomic ratios through iterative age estimation using the ^{230}Th, ^{234}U and ^{238}U decay constants of Jaffey et al. (1971) and Cheng et al. (2013). Since coral reef terraces are subjected to diagenetic processes, the validation of $^{230}Th/^{234}U$ ages has been done by comparison of the initial ratio between ^{238}U and ^{234}U (expressed as $\delta^{234}U$ of the coral with the modern seawater (msw) uranium isotopic composition, that is, $\delta^{234}U(msw) = 146.8 \pm 0.1$ ‰; Andersen et al., 2010).

3.3. Coastal Terrace and Uplift Rate

Sequences of marine and coral reef terraces conveniently permit estimating the upper and middle Pleistocene vertical motion. Uplift rates are calculated from the shoreline angle elevation, its age and its eustatic paleo-sea level elevation (e.g., Murray-Wallace and Woodroffe, 2014; Pedoja et al., 2014; Rovere et al., 2016). The shoreline angle is at the intersection between a terrace flat and its corresponding paleo-sea cliff landwards. Although the relationship is not always straightforward (Pastier et al., 2019), the shoreline angle is assumed to give a statically valid morphological approximation of a period of maximum relative sea-level stands (Lajoie, 1986). In practice, the age of reworked corals sampled in the sinter cover of the fossil notch or/and from the ages of corals in growth position on the part of the coastal terrace help to determine highstands responsible for the final formation of the coastal terrace morphology. These correlations could avoid age discrepancies between the age of coral growth and the age of abandonment of the terrace surface. The morphological growth is affected by multiple processes, marine erosion in particular, which can abrade the uppermost corals and modify the elevation of a morphological surface after the deposition of one or several coral units (e.g., Chauveau et al., 2021). Mean uplift rates are given by dividing the difference between the present elevation of the shoreline angle and the eustatic sea level at its formation time by its age. There is a relative consensus on the succession of the most recent highstands. The most common highstand worldwide in the geomorphological record is the MIS (Marine Isotope Stage) 5 (Creveling et al., 2017; de Gelder et al., 2022; Murray-Wallace & Woodroffe, 2014; Pedoja et al., 2011, 2014; Rovere et al., 2016; Stirling et al., 1998), which includes three relative highstands, MIS 5a (85 ± 5 ka), MIS 5c (100 ± 5 ka), and MIS 5e (122 ± 6 ka). The latest compilations of geomorphic indicators for the variability of sea levels curves of Murray-Wallace and Woodroffe (2014) and Rovere et al. (2016) assign an elevation of 6 ± 4 m with respect to present-day sea level to the MIS5e highstand. Creveling et al. (2017) propose an MIS 5c eustatic highstand of −9.4 ± 5.3 m in agreement with and the most recently evaluated RSL data from Indonesia (de Gelder et al., 2022; Weiss et al., 2022).

4. Results

4.1. Imías

Along the southern coast of Cuba, to the west of the village of Imías, we surveyed a sequence of eight coastal terraces up to a maximum elevation of 160 m (Figures 2 and 3). The DGPS profile evidences the shoreline angles of the three lowest terraces (T1, T2, and T3) at respective elevations of 9 ± 1, 14 ± 1, and 25 ± 1 m. The shoreline angles of the upper terraces (T4, T5, T6, and T7) stand at elevations of 39 ± 1, 52 ± 2, 102 ± 1, and 152 ± 1 m, respectively. The lowermost coastal terrace T1 is made of a lower, 4–5 m thick reefal unit including corals in growth position overlaid in unconformity by a 2 m thick layer of conglomerate made of coral deposits. We dated two corals in growth position from the bioconstructed unit of T1 using U-Th dating (Figure 3 and Table 1). Samples CUB18.4 and CUB18.6 yielded ages of 136 ± 0.7 and 128 ± 0.7 ka, respectively (Figure 3 and Table 1).

4.2. Río Seco

At Río seco, 28 km east of Imías, through dGPS measurements, we estimated the elevation of the shoreline angle of the lower coastal terrace at 15 ± 1 m (Figures 2 and 4). However, in its distal part, locally close to the modern sea cliff, the profile shows a topographic offset at 6 ± 1 m elevation bounding two different units, revealing the existence of a composite terrace (Figure 4). The dated corals on both side of this boundary yielded very different U-Th ages. The upper one, sample CUB18.15 taken in the upper unit, provided an age of 142 ± 0.7 ka whereas sample CUB18.13, sampled in the lower unit, yielded an age above the limit of the method (Table 1). The lowermost terrace T1 is therefore made of a least two distinct reefal limestone units, correlated to two different MIS stages. The upper unit, is only a few meters thick in the modern sea cliff.

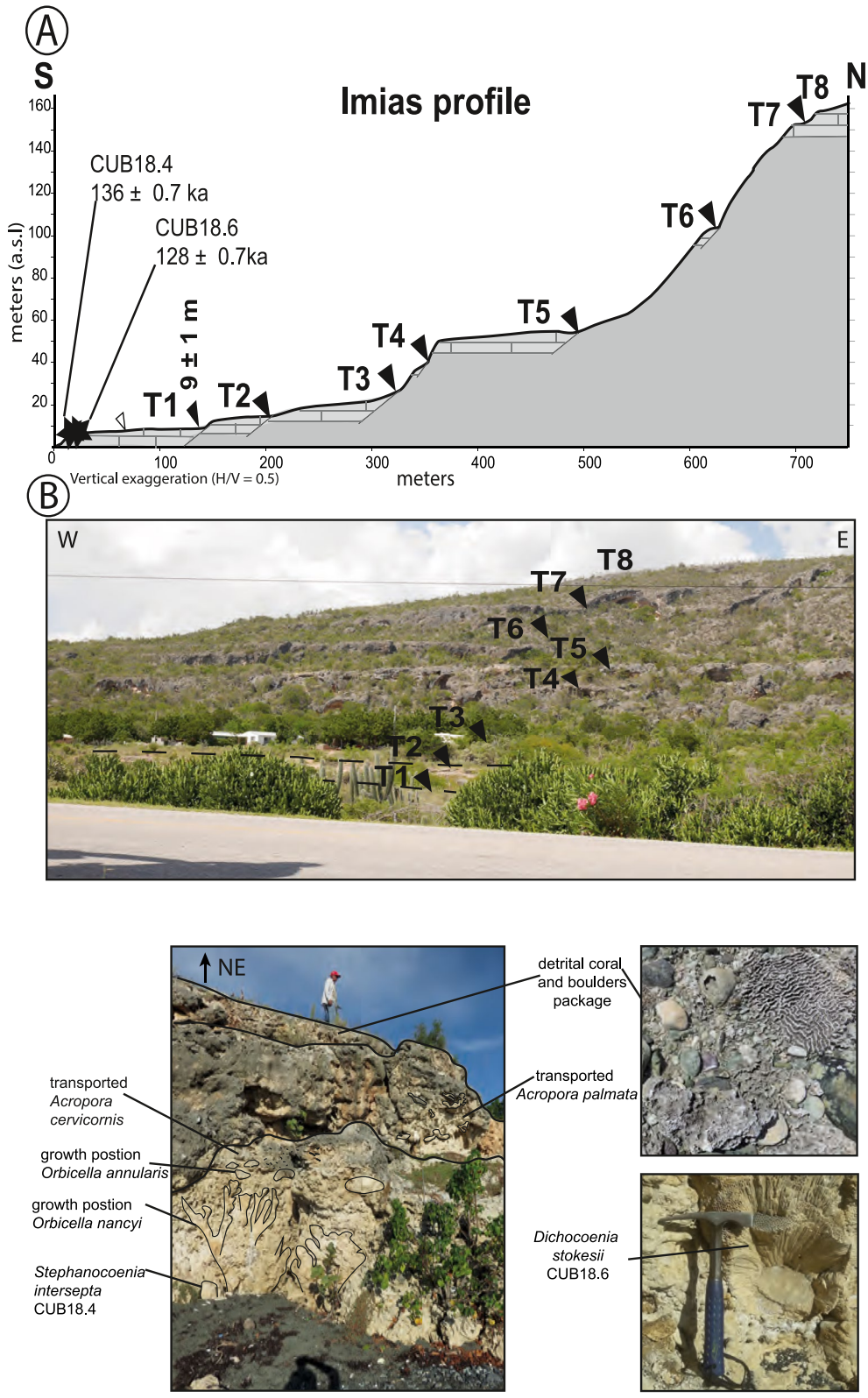

Figure 3. The coastal sequence at Imías. (a) General view (dGPS profile), (b) Interpreted field pictures and sampling details.

Table 1
Samples of Marine Terrace Corals for U/Th Datation

	Sample information					Sample composition	
Samples	Coral species	Morphological location	*Y* (Latitude) (DD)	*X* (Longitude) (DD)	Inner edge elevation (m)	Calcite (%)	Aragonite (%)
CUB18.4	*Stephanocoenia intersepta*	T1 Imias distal edge	20.05167	−74.72883	9 ± 1	<1	>99
CUB18.6	*Dichocoenia stokesii*	T1 Imias distal edge	20.05167	−74.72883	9 ± 1	<1	>99
CUB18.13	*Dichocoenia stokesii*	T1 Rio Seco distal edge	20.07643	−74.40282	15 ± 1	1	99
CUB18.15	*Stephanocoenia intersepta*	T1 Rio Seco distal edge	20.07643	−74.40282	15 ± 1	3	94
CUB18.29	*Stephanocoenia intersepta*	T1 South Maisi distal edge	20.07647	−74.30707	13 ± 1	<1	>99
CUB18.33	*Dichocoenia stokesii*	T1 South Maisi distal edge	20.07647	−74.30707	13 ± 1	3	97
CUB18.35	*Dichocoenia stokesii*	T1 South Maisi distal edge	20.07647	−74.30707	13 ± 1	2	98
CUB18.37	*Pseudodiploria strigosa*	T1 South Maisi inner edge	20.07015	−74.29948	13 ± 1	3	97
CUB18.39	*Dichocoenia stokesii*	T1 South Maisi central part	20.07453	−74.30392	13 ± 1	5	95
CUB18.41	*Dichocoenia stokesii*	T1 South Maisi central part	20.07453	−74.30392	13 ± 1	2	98
CUB18.70	*Colpophyllia natans*	T2 North Maisi inner edge	20.30517	−74.29502	17 ± 1	3	96
CUB18.72	*Dichocoenia stokesii*	T1 North Maisi distal edge	20.30728	−74.29243	17 ± 1	5	95
CUB18.78	*Dichocoenia stokesii*	T1 Cayo Guing inner edge	20.43488	−74.56482	12 ± 1	9	90

4.3. Southern Punta de Maisí

On the southern flank of Punta de Maisí between Playa Blanca and Punta Caleta (Figure 2), we identified 29 coral reef and marine terraces culminating at ∼520 m in elevation (Figure 5). The coastal terraces T1 to T13 are narrower than the coastal terraces T14 to T29 (Figure 6). Some coastal terraces are occasionally discontinuous along some coastal stretches (e.g., T1, T8, T9, T10, T11 and T12), implying the presence of a high topographic escarpment between two of them when some intermediate terraces are absent (Figure 5). Some coastal terraces are separated from each other by a topographic step (paleo-cliff) oblique to the modern coastline (T1 from T2, or T7 from T9) (Figure 5).

The reworked coral sample (CUB18.37) encrusted in the notch associated with the lowest terrace (T1), yielded an U-Th age of 108 ± 0.5 ka (Figure 6, Table 1). CUB18.39 and CUB18.41, were both sampled in coral colonies from the central part of T1, and gave ages of 131 ± 0.6 ka and 118 ± 0.9 ka (Table 1). The three samples taken in the distal edge of T1 provided ages above 300 ka (CUB18.29, CUB18.33, and CUB18.35) (Figure 6, Table 1). In the distal part of the coastal terrace, two units are separated by an unconformity (Figure 6). The lower unit is associated with the three corals dated older than 300 ka. This superposition of discordant units reveals a compound terrace associated with two units, comparable to the structure of the lower terrace at the Rio Seco site, with a thin coral limestone formed during MIS 5 capping an older lower unit.

4.4. Northern Punta de Maisí

East of the Yumurí canyon on the northern flank of Punta de Maisí (Figure 2), the coastal sequence includes nine terraces. The sequence is composed of a low-standing coral reef terrace (T1) separated from the other

^{230}Th/U chemistry							
^{238}U [μg/g]	^{232}Th [ng/g]	(^{234}U/^{238}U)	(^{230}Th/^{238}U)	Age uncorrected [ka]	Age corrected [ka]	Proposed MIS	(^{234}U/^{238}U) initial
2.51 ± 0.01	0.093 ± 0.001	1.10819 ± 0.00045	0.80199 ± 0.00201	135.825 ± 0.677	135.824 ± 0.657	5e	1.15882 ± 0.00070
2.05 ± 0.01	0.229 ± 0.001	1.10920 ± 0.00041	0.77890 ± 0.00224	128.270 ± 0.680	128.267 ± 0.675	5e	1.15692 ± 0.00060
1.89 ± 0.01	0.196 ± 0.001	1.01748 ± 0.00039	1.04675 ± 0.00378	Out of range	Out of range	/	/
2.18 ± 0.01	0.125 ± 0.001	1.12179 ± 0.00049	0.83268 ± 0.00193	142.215 ± 0.668	142.214 ± 0.688	5e	1.18205 ± 0.00080
2.16 ± 0.01	0.668 ± 0.004	1.05929 ± 0.00042	1.09896 ± 0.00243	Out of range	Out of range	/	/
2.45 ± 0.01	0.780 ± 0.004	1.02228 ± 0.00033	1.05299 ± 0.00233	Out of range	Out of range	/	/
2.91 ± 0.02	0.707 ± 0.004	1.01296 ± 0.00027	1.03560 ± 0.00207	Out of range	Out of range	/	/
2.85 ± 0.01	3.044 ± 0.016	1.10330 ± 0.00031	0.70203 ± 0.00184	108.018 ± 0.480	107.991 ± 0.464	5c	1.14017 ± 0.00040
1.88 ± 0.01	0.550 ± 0.003	1.10415 ± 0.00089	0.73925 ± 0.00307	117.828 ± 0.889	117.821 ± 0.892	5e	1.14530 ± 0.00120
2.16 ± 0.01	0.706 ± 0.004	1.10089 ± 0.00050	0.78073 ± 0.00203	130.936 ± 0.664	130.928 ± 0.628	5e	1.14606 ± 0.00070
2.02 ± 0.01	1.044 ± 0.006	1.09429 ± 0.00041	0.73571 ± 0.00199	118.962 ± 0.584	118.949 ± 0.601	5e	1.13197 ± 0.00060
2.01 ± 0.01	0.225 ± 0.001	1.10177 ± 0.00043	0.77256 ± 0.00223	128.157 ± 0.681	128.154 ± 0.702	5e	1.14620 ± 0.00060
2.62 ± 0.01	0.093 ± 0.001	1.10839 ± 0.00040	0.76874 ± 0.00235	125.397 ± 0.706	125.396 ± 0.727	5e	1.15449 ± 0.00060

terraces by a 25-m high paleo-sea cliff (Figure 7). A notch is carved at the foot of the T1 cliff at an elevation of ∼17 m. The notch is karstified and associated with coastal sediments. This sinter cover shelters remobilized corals, one of which has been sampled and dated to 119 ± 0.6 ka (CUB18.70, Table 1). On the distal part of T1, close to the modern coastline, a coral in a growth position has been dated at 128 ± 0.7 ka (CUB 18.72, Figure 7 and Table 1). The CUB 18.70 age and the CUB 18.72 are correlated with MIS 5e sea level highstand but CUB18.72 is older than CUB 18.70. The CUB18.72 in T1 is associated with a constructional phase (coral in growth position) whereas CUB18.70 gives an age of the final coastal terrace geomorphology to T1 (notch formation).

4.5. Cayo Güin

To the northwest of Punta de Maisí, the Cayo Güin site (Figure 2) is associated with a sequence including three successive coastal terraces (Figure 8). The lower marine terrace is limited uphill by a well-marked cliff. The shoreline angle of T1 is raised at 12 ± 1 m in elevation. The fossil sea cliff is notched and accompanied by a sinter cover with reworked corals. One of these corals has been dated at 125 ± 0.7 ka (CUB18.78) that we relate to MIS 5e (Table 1).

5. Discussion

5.1. Estimates of Shoreline Angle Age for Each Lower Terraces

Except for the southern Punta de Maisí site, all the lower terraces dated by U-Th method yield close to MIS 5e either from corals of the upper reef unit, or from reworked corals embedded in notches. We therefore correlate

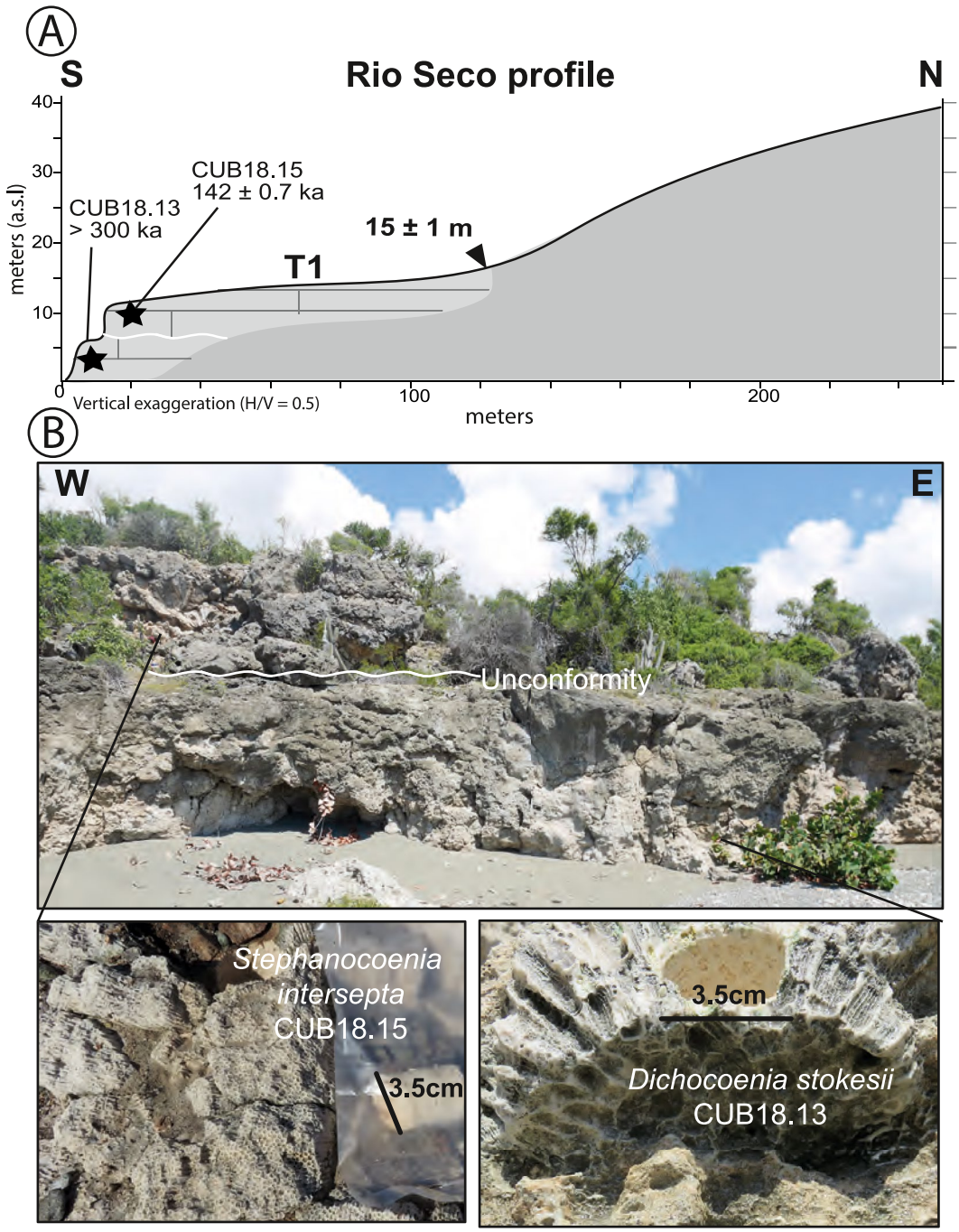

Figure 4. The coastal sequence at Rio Seco. (a) General view (dGPS profile), (b) Interpreted field pictures and sampling details.

these lower terraces with the Last Interglacial (~120–130 ka) as previously done without absolute U-Th dating in this zone (see synthesis in Peñalver et al. (2021)). For the southern Punta de Maisí site, the corals dated from the upper reef unit yielded ages of MIS 5e (CUB 18.39–41), whereas the notch-encrusting coral has an age that can be better correlated to MIS 5c (~100 ka) (CUB 18.37). This lower age corresponds to the timing of notch carving, at a younger age than the lowermost terraces found at other sites that are associated with MIS 5e. This hypothesis is consistent with the presence of a morphological escarpment between the Southern Punta de Maisi lower terrace and the lowest terrace 200 m eastwards, which is higher and continuous along Punta de Maisí, U-Th dated to MIS 5e in Northern Punta de Maisí site (Figures 5 and 7). The lower terrace associated with MIS 5c in the southern

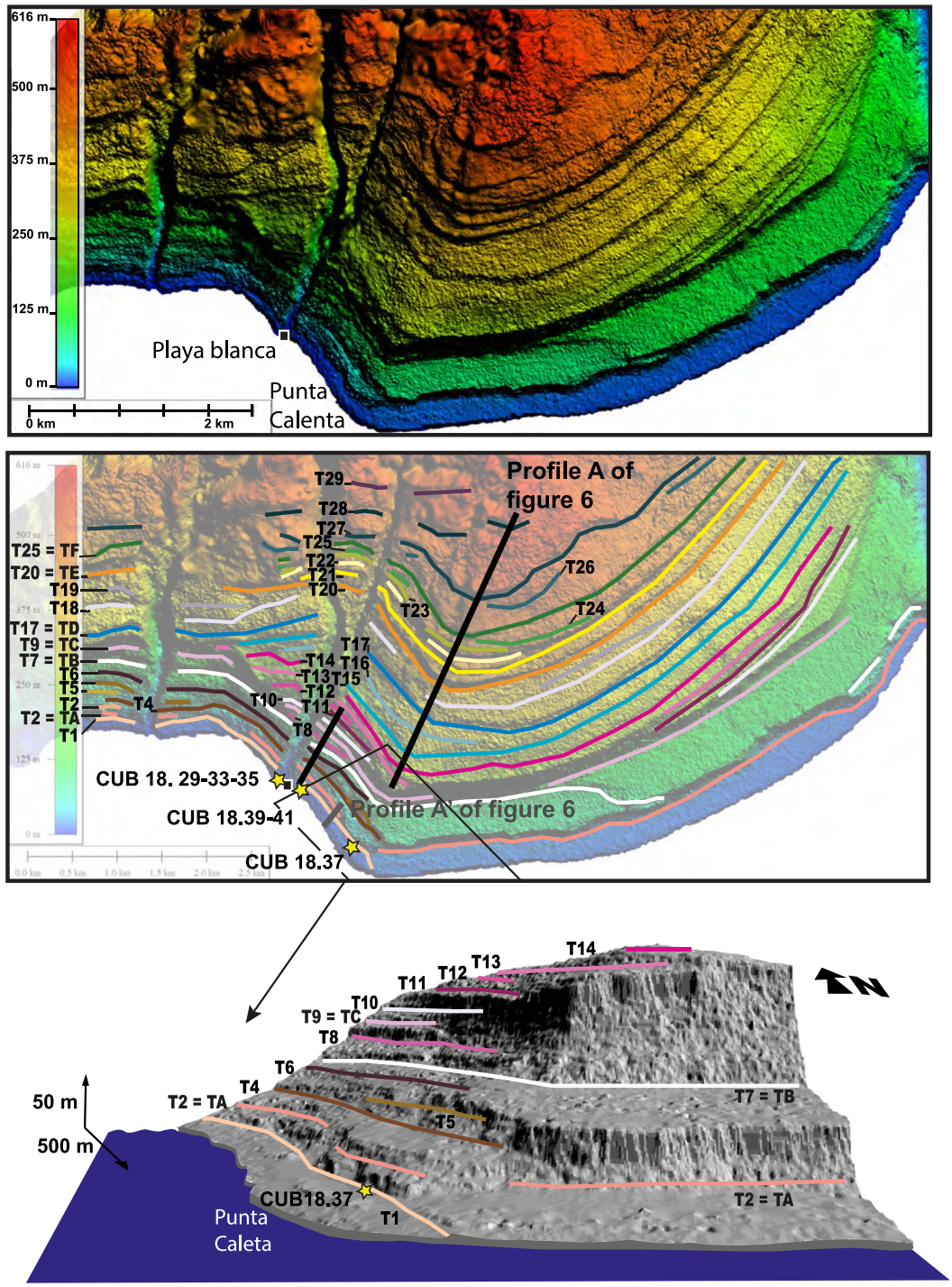

Figure 5. Colored hillshade of high-resolution ALOS Digital Elevation Model (DEM) on the southern Punta de Maisí site (top), interpreted colored hillshade with the location of shoreline angle of coastal terraces in colored lines (middle) and 3D oblique view of a greyscale hillshade of the ALOS DEM, dGPS profile and sampling locations.

Punta de Maisí site below terrace T2 whose 33 m high shoreline angle is close to the shoreline angle of the lower terrace further east (Figure 5). We thus hypothesize that this terrace T2 was formed contemporaneously to the lower terrace further east dated to MIS 5e. The lower terrace of the southern Punta de Maisí site shows similar features to Sumba Island (Cape Laundi) or Haitian coral reef terraces where the ages of several corals sampled on the lower terrace have been associated with both MIS 5c and MIS 5e (Chauveau et al., 2021; Hearty, 2007). This

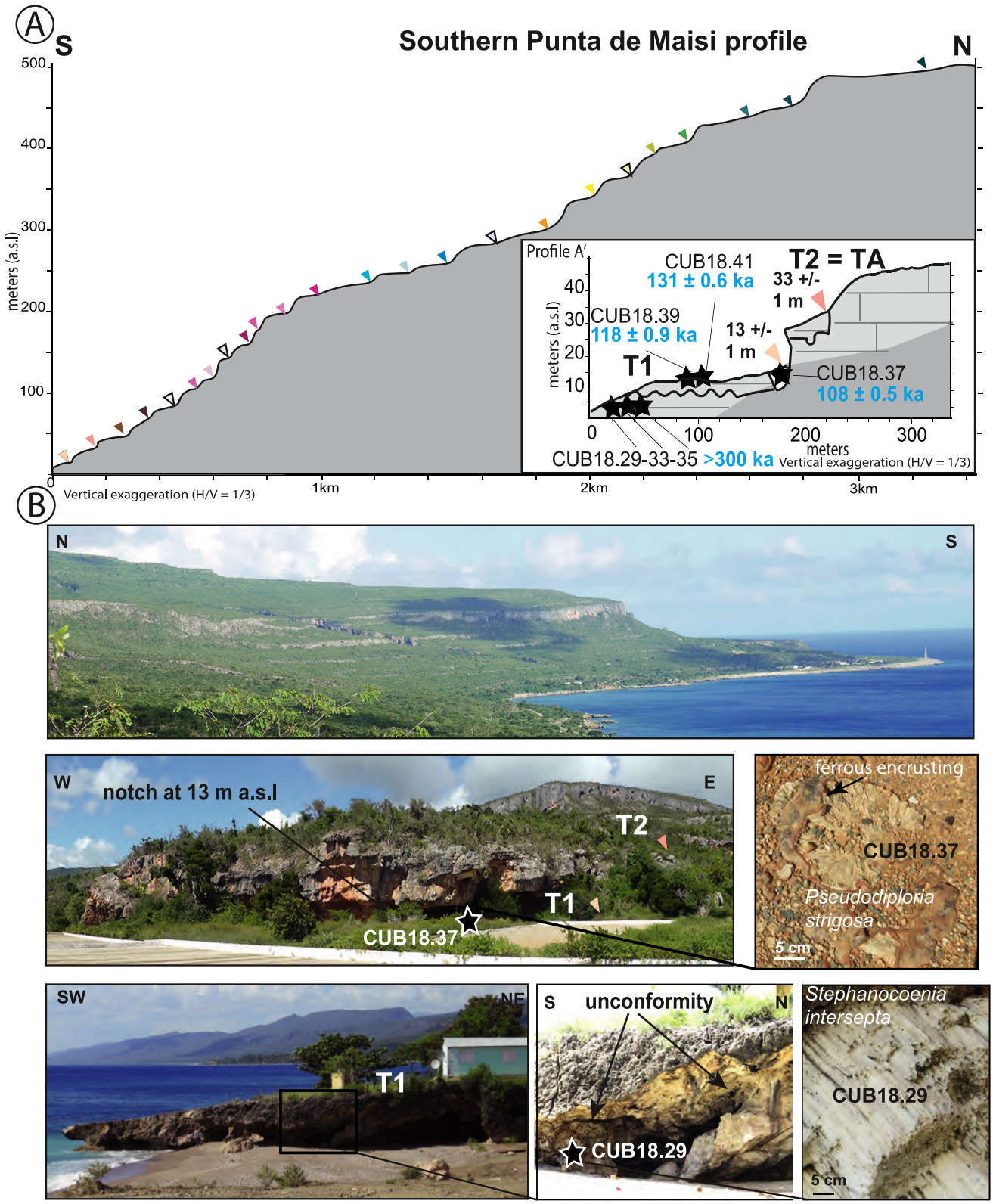

Figure 6. Coastal sequence at the southern Punta de Maisí site. (a) site DGPS profiles, (b) Interpreted field pictures and sampling details.

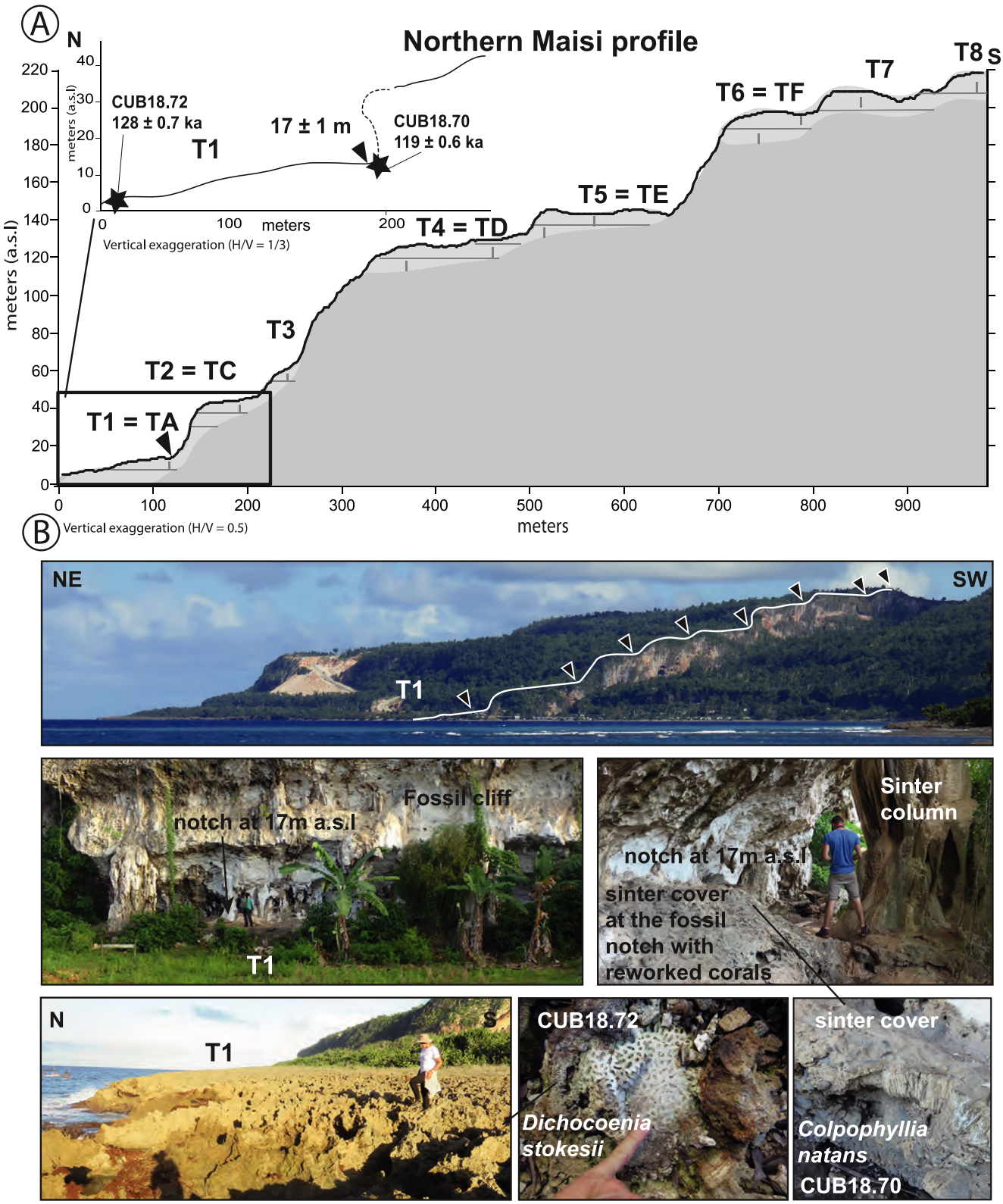

Figure 7. Coastal sequence at Northern Punta de Maisí site. (a) General view (dGPS profile), (b) Interpreted field pictures and sampling details. Arrows indicate the distal edge of each marine terrace.

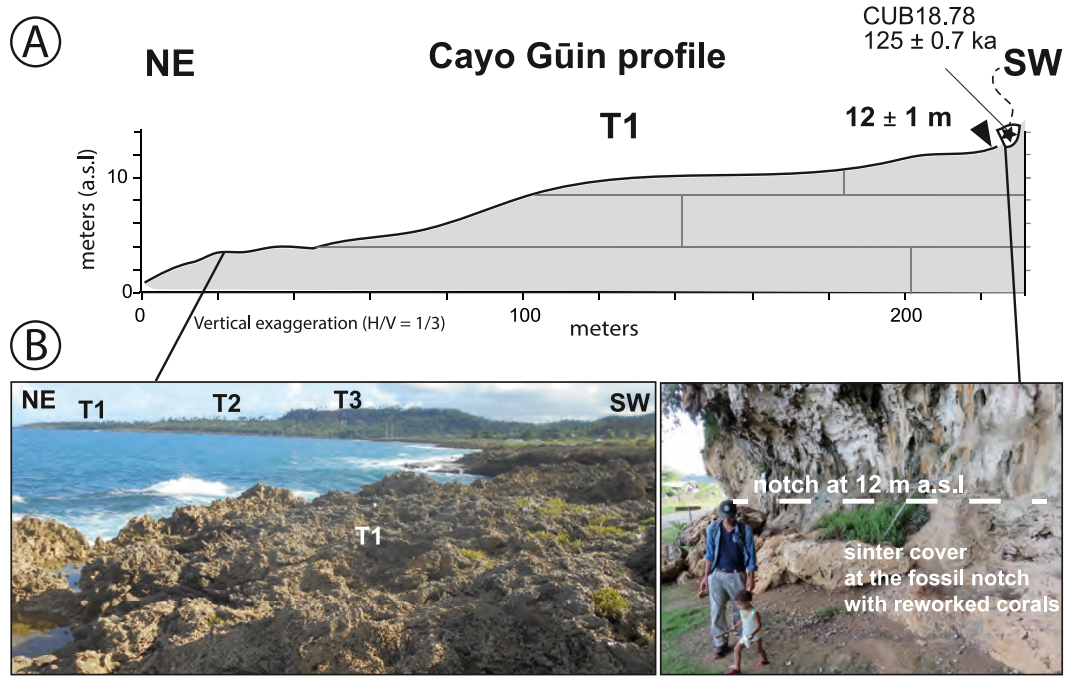

Figure 8. Coastal sequence at Cayo Gūin site. (a) General view (dGPS profile), (b) Interpreted field pictures and sampling details.

exemplifies the fact that the joint effects of marine erosion and reoccupation of older coral terraces at variable uplift rates occasionally challenge the simple assumption of a bijective relationship between sea level stands and coastal terraces, as already pointed by Pedoja et al. (2018) and Pastier et al. (2021).

5.2. Upper Pleistocene Uplift Rates

We derive eustasy-corrected uplift rates from the inner edge elevations of dated marine terraces, once correlated to the nearest interglacial maximum (e.g., de Gelder et al., 2020; Pedoja et al., 2018). In the southern Punta de Maisí site, the uplift rate peaks at 0.23 ± 0.07 mm yr^{-1} or at 0.23 ± 0.06 mm yr^{-1} fromT1 MIS 5c age or T2 MIS 5e age, respectively (table 2). The consistency of uplift rates obtained from T1 or T2 corroborates the assumptions of the correlation between MIS5c/5e and lower marine terraces (T1 = M1S 5c and T2 = MIS 5e) in the southern Punta de Maisí site. This uplift rate corresponds to 3% to 1.6% of the short-term horizontal slip rate of the SOFZ (10 ± 0.1 mm yr^{-1}) (Calais et al., 2016). At Imías, the calculated eustasy-corrected uplift rate is 0.03 ± 0.04 mm yr^{-1} (Table 2). At Río seco, the uplift rate value increases to 0.08 ± 0.04 mm yr^{-1}. To the North, uplift rates increase eastward from 0.05 ± 0.04 mm yr^{-1} at Cayo Güin site, to 0.1 ± 0.05 mm yr^{-1} at the northern Punta de Maisí site. The values obtained for all the five sites of this study agree with the results of Peñalver et al. (2021) that proposed mean eustastic-corrected uplift rates ranging from 0.08 ± 0.04 mm yr^{-1} to 0.28 ± 0.05 mm yr^{-1} according to the lower terrace elevation described on the Maisí area.

Table 2
Uplift Rates Calculated as a Function of Age and Elevation of the Inner Edge of Each Lower Marine Terrace

Marine terrace	MIS age (ka)	Inner edge elevation (m)	Eustatic correction (m)	uplift rate (mm yr^{-1})
T1 Imias	122 ± 6	9 ± 1	6 ± 4 (Murray-Wallace & Woodroffe, 2014)	0.03 ± 0.04
T1 Rio Seco	122 ± 6	15 ± 1	6 ± 4 (Murray-Wallace & Woodroffe, 2014)	0.08 ± 0.04
T1 Southern Maisi	100 ± 5	13 ± 1	−9.4 ± 5.3 (Creveling et al., 2017)	0.23 ± 0.07
T2 Southern Maisi	122 ± 6	33 ± 1	6 ± 4 (Murray-Wallace & Woodroffe, 2014)	0.23 ± 0.06
T2 Northern Maisi	122 ± 6	17 ± 1	6 ± 4 (Murray-Wallace & Woodroffe, 2014)	0.1 ± 0.05
T1 Cayo Guing	122 ± 6	12 ± 1	6 ± 4 (Murray-Wallace & Woodroffe, 2014)	0.05 ± 0.04

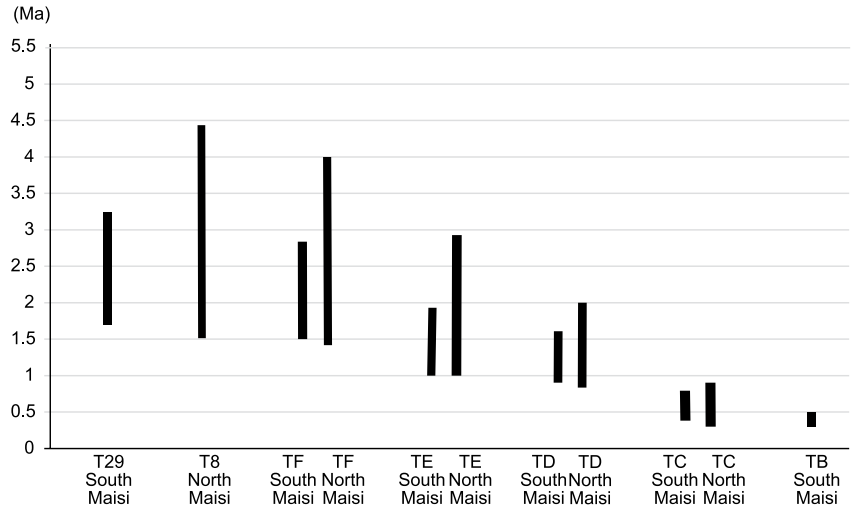

Figure 9. Age range (black column) calculated from the upper Pleistocene uplift rates as derived from ages and inner edge elevations of the reference marine terraces of the southern and northern Punta de Maisí sites.

5.3. Timing of Emersion of the Terrace Sequences

We used the upper Pleistocene uplift rates of the southern (0.23 ± 0.07 mm yr^{-1}) and northern (to 0.1 ± 0.05 mm yr^{-1}) Punta de Maisí sites and assumed a constant uplift rate over time on each site to determine the ages of the upper parts of coastal terrace sequences. The highest coastal terraces are at 520 m (T29) and 220 m (T8) above the current sea level on the southern and northern coasts of Punta de Maisí, respectively (Figures 6 and 7). Using the uplift rate with its uncertainties of the southern Punta de Maisí site and the altitude of T29 of this site, the calculated terrace age ranges between 3.25 and 1.7 Ma. Using the uplift rate of the northern Punta de Maisí site and the altitude of T8 of this site, this marine terrace age ranges between 4.4 and 1.5 Ma (Figure 9 and Table 3). The results suggest that southeastern Cuba began to emerge in the late Pliocene-early Quaternary, which is consistent with previous estimates of del Corral (1944) and more recent paleomagnetic data (at most 4 Ma, Peñalver et al., 2003). The highest reference terrace (TF) is at an elevation of 455 and 200 m south and north of Punta de Maisí, respectively (Figure 10). Based on the upper Pleistocene uplift rates, this terrace has an extrapolated age ranging between 2.8 and 1.5 Ma (southern Punta de Maisí) and 4–1.4 Ma (northern Punta de Maisí) (Figure 9 and Table 3). Likewise, we estimate the age of the TE marine terrace to be between 1.9 and 1 Ma (southern Punta de Maisí) or 2.9 and 1 Ma (northern Punta de Maisí). Marine terrace TD has an age of 1.6–0.9 Ma (southern Punta de Maisí) or 2.5–0.8 Ma (northern Punta de Maisí) and TC has an age of 0.75–0.4 Ma (southern Punta de Maisí) or 0.9–0.3 Ma (northern Punta de Maisí) (Figure 9). The TB terrace is absent at the northern Punta de Maisí site, and its age (0.5–0.3 Ma) can only be calculated from the uplift rate (0.23 ± 0.07 mm yr^{-1}) and the altitude of the shoreline angle (80 m) deduced from the southern Punta de Maisí site. Whichever the uplift rate of the two Punta de Maisí sites used, the age ranges for the same terraces are similar (Figure 9). This result suggests consistent uplift rates for both sites and little temporal change in relative uplift rates at the two sites during the Quaternary.

Table 3
Age Estimates of the Main Upper Marine Terraces

Marine terrace	Uplift rate (mm yr^{-1})	Inner edge elevation (m)	Age (Ma)
Upper terrace South Maisi (T29)	0.23 ± 0.07	520	3.25–1.7
TF South Maisi	0.23 ± 0.07	455	2.8–1.5
TE South Maisi	0.23 ± 0.07	300	1.9–1
TD South Maisi	0.23 ± 0.07	260	1.6–0.9
TC South Maisi	0.23 ± 0.07	120	0.75–0.4
TB South Maisi	0.23 ± 0.07	80	0.5–0.3
Upper terrace North Maisi (T8)	0.1 ± 0.05	220	4.4–1.5
TF North Maisi	0.1 ± 0.05	200	4–1.4
TE North Maisi	0.1 ± 0.05	145	2.9–1
TD North Maisi	0.1 ± 0.05	125	2.5–0.8
TC North Maisi	0.1 ± 0.05	45	0.9–0.3

5.4. Deformation of the Coastal Terraces Sequences

Stacked swath profiles of the topography and the six continuous marine terraces highlight distinct spatial variations of their altitudes (Figure 10). No profile shows a simple tilt of these terraces. An apparent northward long-wavelength tilt of the terraces is visible with folds and vertical offsets in the central part of the NS-trending Central Maisí profile (Figure 10d).

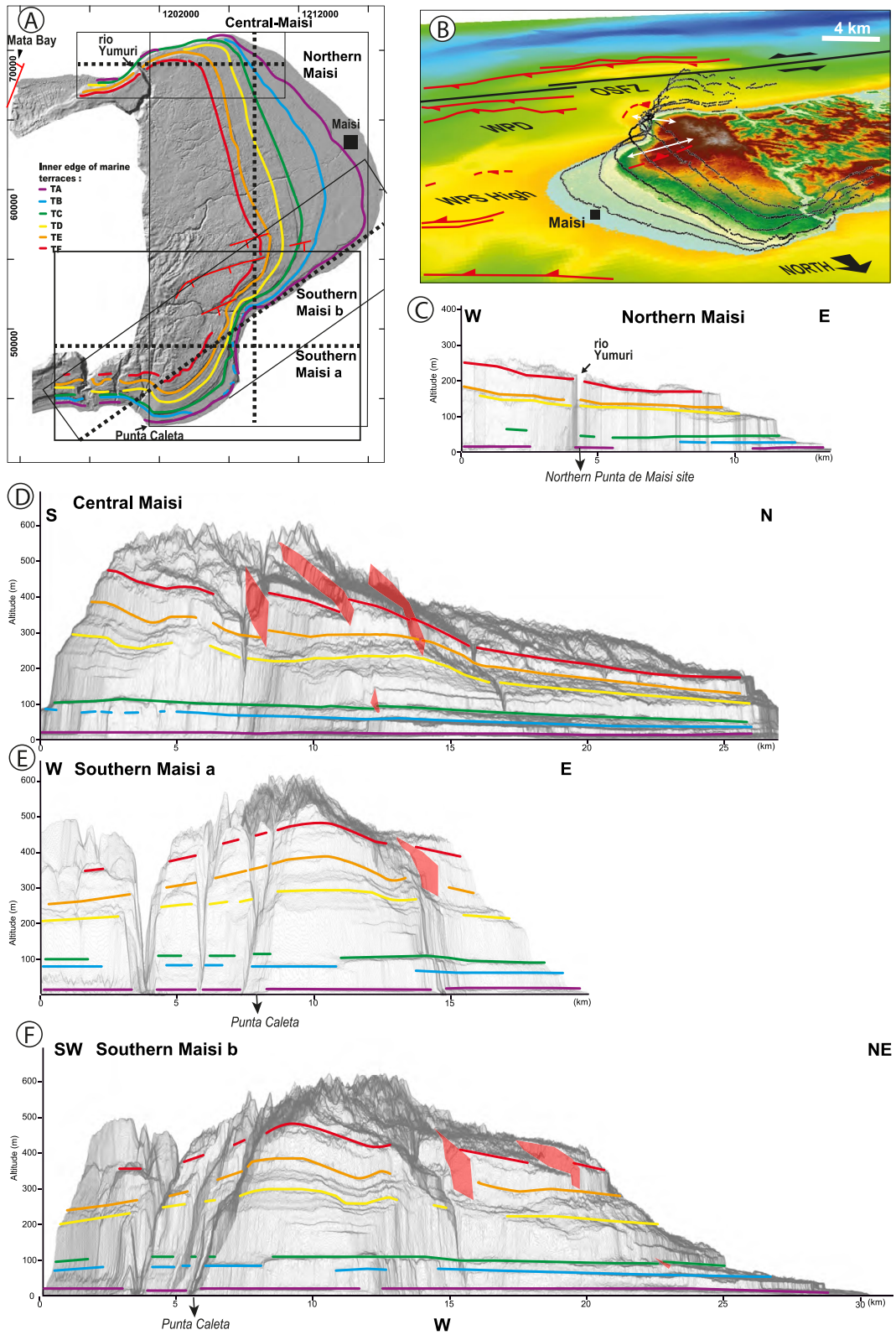

Figure 10. Deformations of long-lasting coastal terrace sequences. (a) Map of the stacked swath profiles of marine terraces in the Punta de Maisí, (b) 3D image of the deformation of the inner edges of continuous marine terraces shown with black lines on 2D image of the Digital Elevation Model. (c) Stacked swath profile of Northern Maisi. (d) Stacked swath profile of Central Maisi. (e) W-E-trending Stacked swath profile of Southern Maisi. (f) SW-NE-trending Stacked swath profile of Southern Maisi.

The folds are generally more developed and the tilt generally steeper for the older and higher terraces. The long-wavelength tilt angle decreases progressively with the terrace level in the sequence. This evolution is consistent with a progressive deformation of the terraces from the emergence of the sequence until present-day. This tilt is also consistent with the spatial configuration of the drainage network that displays an asymmetrical layout with longer rivers in the North than in the South (Figure 2). This tilt indicates a southward increasing uplift gradient active since the beginning of the emersion of the terraces. This activity may be related to the vertical component of the transform system or by deformation related to secondary reverse or transpressive faults close to southern coast of the Punta de Maisí (Figure 10b).

The NS-trending Central Maisí profile also highlights several folds of the high terraces from TF to TD decreasing with younger terrace ages (Figure 10d) and becoming inexistent for the youngest terraces. Folding therefore predates TC, which has an extrapolated age ranging of 0.9 to 0.3 Ma. The asymmetry of the folds suggests an apparent north-verging fold system, similar to that of the North Hispaniola reverse fault (Escuder-Viruete and Pérez, 2020; Oliveira de Sá et al., 2021). Vertical offsets are well observed on TF, TE, TD, and TC and characterize normal fault movements with footwalls to the South. The DEM shows that these ENE-trending normal faults do not affect the two lower reference terraces TB and TA, that we assume younger than 0.5–0.3 ka (Figure 10). The south-verging normal fault activity is older than Upper Pleistocene, and could be gravitational according to their curved shapes and the presence of similar structures in the eastern offshore zone (Oliveira de Sá et al., 2021) (Figure 10a).

On the western part of the EW profile of northern Maisí (Figure 10c), the terraces from TF to TC are simply tilted in an apparent eastward direction with similar slope regardless of the age of the terrace. This result indicates a late tilt of these terraces, after the formation of the TC marine terrace but before the formation of the untilted TA marine terrace, that is, between 0.9 and 0.3 and 0.12 Ma. This tilting could be produced by a W-verging normal fault located west of the terraces and running through Mata Bay (Figures 10a and 11). The EW profile of the southern Punta de Maisí zone (Southern Maisí a, Figure 10e) shows that TF, TE, and TD terraces are at high elevations (between 220 and 520 m) and are folded by a short-wavelength anticline. The fold axis is located east of Punta Caleta (Figure 10e). By projecting the elevation of the terrace inner edges along various strikes, we determine that the NE-SW strike projection (Southern Maisí b) shows the maximal flexure east of Punta Caleta with the shortest wavelength and without artifact (Figure 10f). This strike could be perpendicular to a potential NW-SE-trending anticlinal axis (Figure 10b). The NE-SW profile also allows a better appreciation of the asymmetric shape of the fold consistent with SW shearing in agreement with a sinistral transpressive regime and a NE-SW-trending maximum horizontal compressive stress close to the EW-trending transform plate boundary (Moreno et al., 2002).

5.5. Onshore/Offshore Deformation Pattern

Punta de Maisí is the western extension of the Windward Passage Sill of the Septentrional block (Oliveira de Sá et al., 2021; Rodríguez-Zurrunero et al., 2020) (Figures 1 and 11). According to our interpretation, its emersion began between the upper Pliocene and the lower Pleistocene (4.4–1.5 Ma) in agreement with the last transpressional deformation event produced by the oblique collision of the Bahamas platform that uplifted the Windward Passage Sill (Escuder-Viruete et al., 2020; Oliveira de Sá et al., 2021). These deformations occurred just after the activation of the eastern part of the OSFZ north of the Hispaniola block during the Pliocene (Calais & De Lépinay, 1995; Calais et al., 2016; Escuder-Viruete et al., 2020; Le Roy et al., 2015). The analysis of the topographic profiles of the continuous Pleistocene coastal terraces and uplift rates obtained in the five study sites argue that faults and folds have deformed the coastal sequences during the Pleistocene. The north verging fold in the central part of Punta de Maisí agrees with the offshore folding north and East of the Punta de Maisí (Oliveira de Sá et al., 2021). Underthrusting of the Bahamas Platform north of the Punta de Maisí below the northwestern prolongation of the Northern Hispaniola Fault Zone could produce this deformation in the upper plate (Oliveira de Sá et al., 2021). The NW-trending anticline on the southern coast of the Punta de Maisí is better explained by the transpressional tectonic regime close to the transform boundary (Oliveira de Sá et al., 2021), which is widespread in the Hispaniola block south of the SOFZ (e.g., in the Jamaica Passage, Corbeau et al., 2016). The results also indicate that uplift rates are increasing toward the SE. This southeastern gradient uplift agrees with more active deformation toward the plate boundary as shown by the shallow seismicity clustered in the southern margin of Cuba (Oliveira de Sá et al., 2021; Rodríguez-Zurrunero et al., 2020). This tectonic pattern points to the prevailing

impact of shortening toward the Septentrional Oriente faut zone. We suggest that the high coupling between the Septentrional block and the Bahamas Platform along the Northern Hispaniola Fault during oblique collision transfers the main part of the shortening southward.

However, the Late Pleistocene uplift rate of the northern Punta de Maisí site (as high as 0.1 ± 0.05 mm yr^{-1}). Together with the north-verging folds affecting the older coastal terraces, could be associated with the western prolongation of the inverse North Hispaniola Fault Zone and/or secondary faults and folds observed in the surrounding submarine domain (Oliveira de Sá et al., 2021; Rodríguez-Zurrunero et al., 2020) (Figure 11). This western fault segment reactivates the structures of the Cretaceous Caribbean arc/North American suture zone, and likely continues propagating to the Northwest. To the NW of the study zone, an historical earthquake of 5.4 of magnitude in 1988 was correlated with this segment (Figure 1) and a seismic profile has shown sediments incorporated into an associated narrow fold-and-thrust imbricate system (Figure 17 in Rodríguez-Zurrunero et al., 2020 and Figure 10 in our study).

The westernmost sites of this study (i.e., Imías and Cayo Gūin sites) show moderate uplift rates compared to the values of the eastern sites. The westward decreasing uplift rate observed in the northern coast is consistent with the NW-dipping normal faults near Baracoa and 15 km southwards (Figure 11), which discontinuously reduce uplift rates westward and explains the deformation pattern of the oldest terraces in the northern Punta de Maisí (see Section 4.3). We propose that this westward uplift rate decrease is related to the westward decrease of activity along the Northern Hispaniola Fault Zone. The underthrusting of the Bahamas Platform is more or less blocked westward below the fault zone and oblique collision is thus mostly accommodated elsewhere (Rodríguez-Zurrunero et al., 2020). Calais and de Lepinay (1991), Calais et al. (1998), and Enman et al. (1997), defined the Santiago Deformed Belt southwest of the study zone and south of the SOFZ (Figure 1). They interpreted this structure as an active compressive area extending along the southern margin of Cuba. They related this E-W trending belt to transpressional deformation due to oblique motion along the SOFZ. This belt accommodates a part of the Bahamas Platform shortening in this area. The westward locking of the Bahamas Platform underthrust beneath the North Hispaniola Fault Zone may be related to the northwestward transition from thick oceanic to the continental crust of the Bahamas (Ladd & Sheridan, 1987; Uchupi et al., 1971) which can no longer underthrust under Cuba (Figure 1). The oblique collision is thus accommodated further south at the current plate boundary that currently separates the ancient Cretaceous-Paleogene Cuban arc to the north from the Gonave block to the south (Oliveira de Sá et al., 2021). The zone under the Santiago Deformed Belt, could correspond to the transition between the continental and the oceanic crust of the Eocene passive margin associated with the Mid-Cayman Through ridge (Leroy et al., 1996; Figure 1). This transitional crust could allow the Gonave block to underthrust more easily the ancient Cretaceous-Paleogene Arc of Cuba at the North Caribbean Plate boundary (SOFZ and Santiago Deformed Belt) as suggested by seismicity around this tectonic boundary (Moreno et al., 2002; Figure 8 in Rodríguez-Zurrunero et al., 2020).

Last, the Beata Ridge south of Hispaniola Island could also partly explain the EW-trending variation of the uplift of the southeastern tip of Cuba (Figure 1). The Beata Ridge was interpreted as an indenter formed of a 15-km thick Caribbean oceanic crust that has increased the shortening between the Hispaniola block and the Bahamas Platform since the early Miocene or Early Pliocene (Ewing et al., 1960; Huerta & Pérez-Estaun, 2002; Mauffret & Leroy, 1997, 1999; Pubellier et al., 2000; Terence Edgar et al., 1971; Vila et al., 1990) (Figure 1). The terraces of the Punta de Maisí would therefore record in part the EW-trending deformation gradient produced by this indentor.

6. Conclusion

During the end of the Pliocene, the geodynamics of the North American and Caribbean plates boundary changed with the onset of the Bahamas-Hispaniola collision and the activation of the strike-slip Septentrional fault of the SOFZ (Calais et al., 2016; Oliveira de Sà et al., 2021). To the North of the OSFZ, the North Hispaniola Fault Zone accommodates the south-verging underthrusting of the Bahamas Platform. The Quaternary deformation across the southeastern tip of Cuba (Punta de Maisí) determined from the marine and coral reef terraces analyses mirrors this large-scale geodynamics evolution. The Punta de Maisí belongs to the Septentrional block between the SOFZ and the North Hispaniola Fault Zone. The estimated age of the sequences of coastal terraces indicates that Punta de Maisí continuously uplifts at least since the late Pliocene emersion. These coastal terrace sequences are the highest and most developed in Cuba. North-verging shearing of the Septentrional block produced by the south-verging

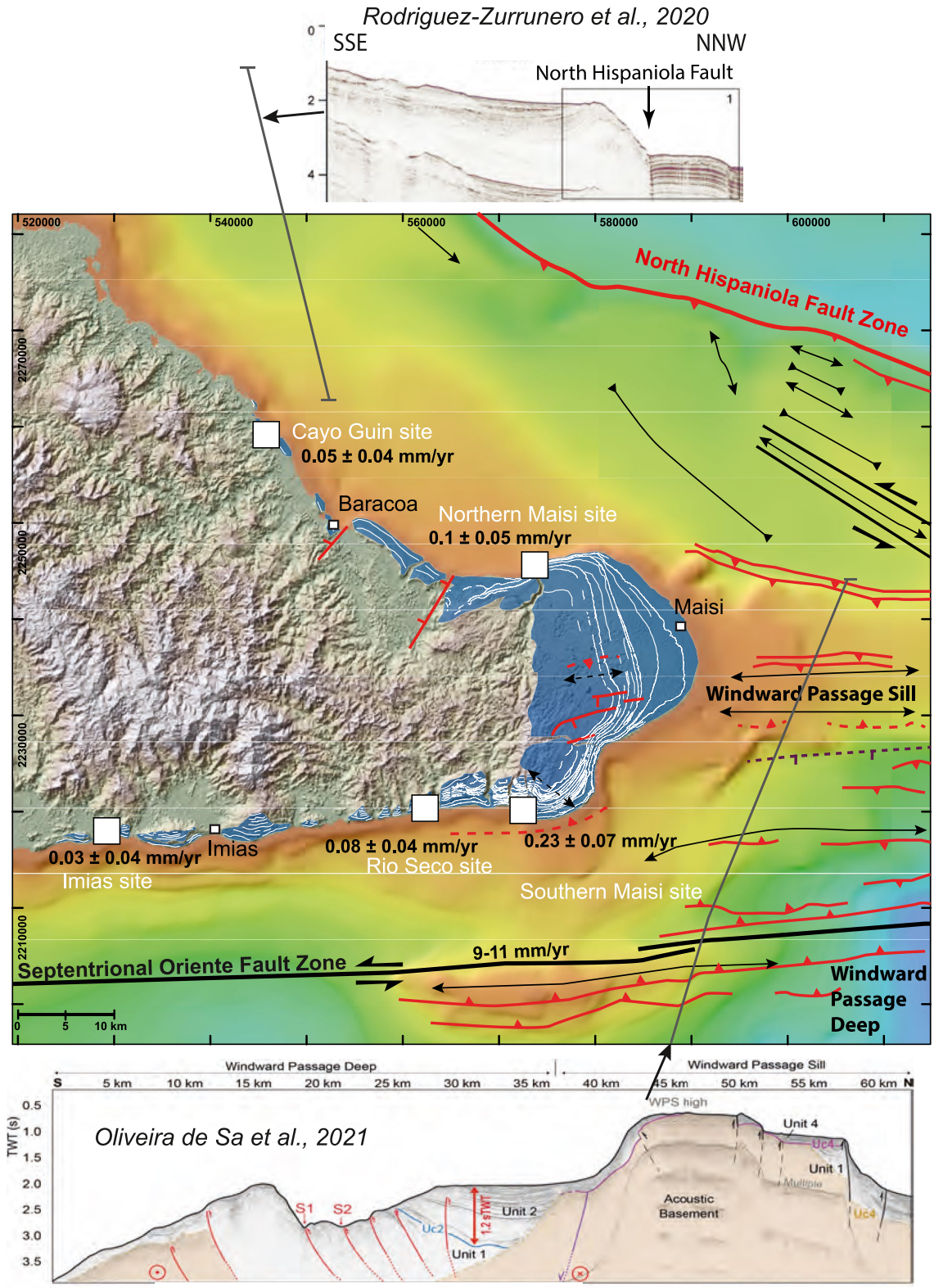

Figure 11. Marine terrace boundaries (White) and onshore uplift rates at sampled sites (squares) (our study); offshore structural map and seismic profiles from Leroy et al. (2015), Rodríguez-Zurrunero et al. (2020), and Oliveira de Sá et al. (2021).

underthrusting of the Bahamas affects the upper marine terraces. Uplift reaches its maximal rates near the SOFZ (Late Pleistocene uplift rate of 0.23 ± 0.07 mm yr^{-1}) and decreases westward. We interpret this lateral variation with a locking of the Bahamas underthrusting under the North Hispaniola Fault Zone due to a westward increasing coupling across the fault interface and a transfer of shortening south of the SOFZ on the Santiago Deformed Belt.

Data Availability Statement

The topographic data (longitude, latitude coverage of −74,40°; 20,30° and −74,09°; 20,06°) used in this study is available at: http://www.latitude-geosystems.com [Dataset]. Pleiades CNES stereoscopic satellite images are available at: https://dinamis.teledetection.fr [Dataset]. The ESRI's ArcGIS 10 software is available at: https://www.esri.com [Software]. U/Th data are integrated into the manuscript in Table 1. Uplift rates and coastal terrace ages were calculated from this data and elevation values are indicated in Tables 2 and 3. All these figures and tables can also be found online via Zenodo (https://zenodo.org/badge/DOI/10.5281/zenodo.8199685.svg; Authemayou, 2023).

Acknowledgments
Denis Scholz is thankful to the DFG for funding (SCHO 1274/11e1 and INST 247/889-1 FUGG). We acknowledge Michael Weber for the U-Th dating with the Thermo Fisher Scientific Neptune Plus MC-ICP-MS in the University of Mainz. This work was supported by public funds received in the framework of GEOSUD (DINAMIS), a project (ANR-10-EQPX-20) of the program "Investissements d'Avenir" managed by the French National Research Agency. It was also supported by the ISblue project, Interdisciplinary graduate school for the blue planet (ANR-17-EURE-0015) and co-funded by a grant from the French government under the program "Investissements d'Avenir" embedded in France 2030 (VuCoRem project, C. Authemayou) and the CNES TOSCA program (CETTROPICO, C. Authemayou).

References

Agassiz, A. (1894). *A reconnoissance of the Bahamas and of the elevated reefs of Cuba in the steam yacht" wild duck", January to April, 1893* (Vol. 26). Museum.

Andersen, M. B., Stirling, C. H., Potter, E. K., Halliday, A. N., Blake, S. G., McCulloch, M. T., et al. (2010). The timing of sea-level high-stands during marine Isotope stages 7.5 and 9: Constraints from the uranium-series dating of fossil corals from Henderson Island. *Geochimica et Cosmochimica Acta*, *74*(12), 3598–3620. https://doi.org/10.1016/j.gca.2010.03.020

Armijo, R., Lacassin, R., Coudurier-Curveur, A., & Carrizo, D. (2015). Coupled tectonic evolution of Andean orogeny and global climate. *Earth-Science Reviews*, *143*, 1–35. https://doi.org/10.1016/j.earscirev.2015.01.005

Authemayou, C. (2023). Oblique collision of the Bahamas Platform at the northern boundary of the Caribbean plate recorded by the Late Cenozoic coastal terraces of SE Cuba [Database]. Zenodo. https://doi.org/10.5281/zenodo.8199685.svg

Boschman, L. M., van Hinsbergen, D. J., Torsvik, T. H., Spakman, W., & Pindell, J. L. (2014). Kinematic reconstruction of the Caribbean region since the Early Jurassic. *Earth-Science Reviews*, *138*, 102–136. https://doi.org/10.1016/j.earscirev.2014.08.007

Burke, K. (1988). Tectonic evolution of the Caribbean. *Annual Review of Earth and Planetary Sciences*, *16*(1), 201–230. https://doi.org/10.1146/annurev.ea.16.050188.001221

Busto, R. D. (1975). *Las terrazas marinas de Maisí. Ciencias Serie 7 Geografía*. Centro de Información Científica y Técnica. Universidad de La Habana.

Cabrera, M., & Peñalver, L. L. (2001). Contribución a la estratigrafía de los depósitos cuaternarios de Cuba. *Revista Cuaternario y Geomorfología*, *15*(3–4), 37–49.

Calais, E., Béthoux, N., & de Lépinay, B. M. (1992). From transcurrent faulting to frontal subduction: A seismotectonic study of the northern Caribbean plate boundary from Cuba to Puerto Rico. *Tectonics*, *11*(1), 114–123. https://doi.org/10.1029/91tc02364

Calais, E., & de Lepinay, B. M. (1991). From transtension to transpression along the northern Caribbean plate boundary off Cuba: Implications for the recent motion of the Caribbean plate. *Tectonophysics*, *186*(3–4), 329–350. https://doi.org/10.1016/0040-1951(91)90367-2

Calais, E., & De Lépinay, B. M. (1995). Strike-slip tectonic processes in the northern Caribbean between Cuba and Hispaniola (Windward passage). *Marine Geophysical Researches*, *17*(1), 63–95. https://doi.org/10.1007/bf01268051

Calais, E., Mazabraud, Y., Mercier de Lépinay, B., Mann, P., Mattioli, G., & Jansma, P. (2002). Strain partitioning and fault slip rates in the northeastern Caribbean from GPS measurements. *Geophysical Research Letters*, *29*(18), 3–1. https://doi.org/10.1029/2002gl015397

Calais, E., Perrot, J., & de Lépinay, B. M. (1998). Strike-slip tectonics and seismicity along the northern Caribbean plate boundary from Cuba to Hispaniola. *Geological Society of America Special Papers*, *326*, 125–169.

Calais, E., Symithe, S., de Lepinay, B. M., & Prépetit, C. (2016). Plate boundary segmentation in the northeastern Caribbean from geodetic measurements and Neogene geological observations. *Comptes Rendus Geoscience*, *348*(1), 42–51. https://doi.org/10.1016/j.crte.2015.10.007

Chauveau, D., Authemayou, C., Pedoja, K., Molliex, S., Husson, L., Scholz, D., et al. (2021). On the generation and degradation of emerged coral reef terrace sequences: First cosmogenic 36Cl analysis at Cape Laundi, Sumba Island (Indonesia). *Quaternary Science Reviews*, *269*, 107144. https://doi.org/10.1016/j.quascirev.2021.107144

Cheng, H., Edwards, R. L., Shen, C. C., Polyak, V. J., Asmerom, Y., Woodhead, J., et al. (2013). Improvements in 230Th dating, 230Th and 234U half-life values, and U–Th isotopic measurements by multi-collector inductively coupled plasma mass spectrometry. *Earth and Planetary Science Letters*, *371*, 82–91. https://doi.org/10.1016/j.epsl.2013.04.006

Corbeau, J., Rolandone, F., Leroy, S., Guerrier, K., Keir, D., Stuart, G., et al. (2017). Crustal structure of western Hispaniola (Haiti) from a teleseismic receiver function study. *Tectonophysics*, *709*, 9–19. https://doi.org/10.1016/j.tecto.2017.04.029

Corbeau, J., Rolandone, F., Leroy, S., Meyer, B., Mercier de Lépinay, B., Ellouz-Zimmermann, N., & Momplaisir, R. (2016). How transpressive is the northern Caribbean plate boundary? *Tectonics*, *35*(4), 1032–1046. https://doi.org/10.1002/2015tc003996

Creveling, J. R., Mitrovica, J. X., Clark, P. U., Waelbroeck, C., & Pico, T. (2017). Predicted bounds on peak global mean sea level during marine isotope stages 5a and 5c. *Quaternary Science Reviews*, *163*, 193–208. https://doi.org/10.1016/j.quascirev.2017.03.003

Crosby, W. O. (1883). Elevated coral reefs of Cuba. *Annals and Magazine of Natural History*, *12*(70), 283–284. https://doi.org/10.1080/00222938309459630

Cruz-Orosa, I., Sàbat, F., Ramos, E., & Vázquez-Taset, Y. M. (2012). Synorogenic basins of central Cuba and collision between the Caribbean and North American plates. *International Geology Review*, *54*(8), 876–906. https://doi.org/10.1080/00206814.2011.585031

D'Angeli, I. M., Sanna, L., Calzoni, C., & De Waele, J. (2015). Uplifted flank margin caves in telogenetic limestones in the Gulf of Orosei (Central-East Sardinia—Italy) and their palaeogeographic significance. *Geomorphology*, *231*, 202–211. https://doi.org/10.1016/j.geomorph.2014.12.008

de Gelder, G., Husson, L., Pastier, A. M., Fernández-Blanco, D., Pico, T., Chauveau, D., & Pedoja, K. (2022). High interstadial sea levels over the past 420ka from the Huon Peninsula, Papua New Guinea. *Communications Earth & Environment*, *3*(1), 256. https://doi.org/10.1038/s43247-022-00583-7

de Gelder, G., Jara-Munoz, J., Melnick, D., Fernández-Blanco, D., Rouby, H., Pedoja, K., et al. (2020). How do sea-level curves influence modeled marine terrace sequences? *Quaternary Science Reviews*, *229*, 106132. https://doi.org/10.1016/j.quascirev.2019.106132

del Corral, J. I. (1944). Terrazas pleistocénicas cubanas. Imp. Compañía editora de libros y folletos.

DeMets, C., Jansma, P. E., Mattioli, G. S., Dixon, T. H., Farina, F., Bilham, R., et al. (2000). GPS geodetic constraints on Caribbean-North America plate motion. *Geophysical Research Letters*, *27*(3), 437–440. https://doi.org/10.1029/1999gl005436

de Neira, J. D., Braga, J. C., Mediato, J., Lasseur, E., Monthel, J., Hernaiz, P. P., et al. (2015). Plio–Pleistocene palaeogeography of the Llanura Costera del Caribe in eastern Hispaniola (Dominican Republic): Interplay of geomorphic evolution and sedimentation. *Sedimentary Geology*, *325*, 90–105. https://doi.org/10.1016/j.sedgeo.2015.05.008

Dentzer, J., Pubellier, M., Ellouz-Zimmermann, N., Amilcar, H. C., Amilcar, H., Momplaisir, R., & Boisson, D. (2021). From neogene thin-skin to recent thick-skin deformation in Haiti fold-and-thrust belt (Western Hispaniola). *Journal of Structural Geology*, *151*, 104414. https://doi.org/10.1016/j.jsg.2021.104414

De Waele, J., D'Angeli, I. M., Bontognali, T., Tuccimei, P., Scholz, D., Jochum, K. P., et al. (2018). Speleothems in a north Cuban cave register sea-level changes and Pleistocene uplift rates. *Earth Surface Processes and Landforms*, *43*(11), 2313–2326. https://doi.org/10.1002/esp.4393

Díaz, I., Rueda, J., Bernal, C., Cabellos, J., Ma, I.-V., Castro, L., et al. (2011). *El movimiento vertical actual de las costas cubanas*. Memorias de la Convención de Informática, Palacio Convenciones.

Díaz, J. L., Magáz, A., Hernández, J., Venero, A., & Pérez, F. (1991). *Reconstrucción tectónica local mediante el análisis de la morfoescultura marina en la franja costera Río Seco-Punta Maisí, provincia de Guantánamo, Cuba. Morfotectónica de Cuba oriental* (pp. 10–19). Editorial Academia.

Dillon, W. P., Edgar, N. T., Parson, L. M., Scanlon, K. M., Driscoll, G. R., & Jacobs, C. L. (1993). *Magnetic anomaly map of the central Cayman Trough, northwestern Caribbean Sea (No. 2083-B)*. US Geological Survey.

Dodge, R. E., Fairbanks, R. G., Benninger, L. K., & Maurrasse, F. (1983). Pleistocene sea levels from raised coral reefs of Haiti. *Science*, *219*(4591), 1423–1425. https://doi.org/10.1126/science.219.4591.1423

Dolan, J. F. & Mann, P. (Eds.) (1998). *Active strike-slip and collisional tectonics of the northern Caribbean plate boundary zone* (Vol. 326). Geological Society of America.

Dumas, B., Hoang, C. T., & Raffy, J. (2006). Record of MIS 5 sea-level highstands based on U/Th dated coral terraces of Haiti. *Quaternary International*, *145*, 106–118. https://doi.org/10.1016/j.quaint.2005.07.010

Enman, S. V., Belousov, T. P., Marquez Tablon, M. E., Rueda Perez, J. S., & Jorge, G. D. (1997). Recent crustal movements and morphostructural pattern of southeastern Cuba: Santiago de Cuba geodynamic research site. *Izvestiya - Physics of the Solid Earth*, *33*(1), 55–69.

Escuder-Viruete, J., Beranoaguirre, A., Valverde-Vaquero, P., & McDermott, F. (2020). Quaternary deformation and uplift of coral reef terraces produced by oblique subduction and underthrusting of the Bahama Platform below the northern Hispaniola forearc. *Tectonophysics*, *796*, 228631. https://doi.org/10.1016/j.tecto.2020.228631

Ewing, J., Antoine, J., & Ewing, M. (1960). Geophysical measurements in the western Caribbean Sea and in the Gulf of Mexico. *Journal of Geophysical Research*, *65*(12), 4087–4126. https://doi.org/10.1029/jz065i012p04087

Furrazola-Bermūdez, G., Judoley, C. M., Mijailovskaya, M. S., Miroliubov, Y. S., Novojatsky, I. P., Nunez-Jimenez, A., & Solsona, J. B. (1964). Geologia de Cuba: La Habana, Inst. Cubano Recursos Minerales (Vol. 239).

Gibert, L., Scott, G. R., Scholz, D., Budsky, A., Ferràndez, C., Ribot, F., et al. (2016). Chronology for the Cueva Victoria fossil site (SE Spain): Evidence for early Pleistocene Afro-Iberian dispersals. *Journal of Human Evolution*, *90*, 183–197. https://doi.org/10.1016/j.jhevol.2015.08.002

Gordon, M. B., Mann, P., Cáceres, D., & Flores, R. (1997). Cenozoic tectonic history of the North America-Caribbean plate boundary zone in western Cuba. *Journal of Geophysical Research*, *102*(B5), 10055–10082. https://doi.org/10.1029/96jb03177

Hearty, P. J., Hollin, J. T., Neumann, A. C., O'Leary, M. J., & McCulloch, M. (2007). Global sea-level fluctuations during the Last Interglaciation (MIS 5e). *Quaternary Science Reviews*, *26*(17–18), 2090–2112. https://doi.org/10.1016/j.quascirev.2007.06.019

Hill, R. T. (1895). *Notes on the Geology of the Island of Cuba: Based upon a reconnoissance made for Alexander Agassiz*. Museum.

Horsfield, W. T. (1975). Quaternary vertical movements in the Greater Antilles. *Geological Society of America Bulletin*, *86*(7), 933–938. https://doi.org/10.1130/0016-7606(1975)86<933:qvmitg>2.0.co;2

Huerta, P. H., & Pérez-Estaun, A. (2002). Estructura del cinturón de pliegues y cabalgamientos de Peralta, República Dominicana. *Acta Geologica Hispanica*, 183–205.

Husson, L., Pastier, A. M., Pedoja, K., Elliot, M., Paillard, D., Authemayou, C., et al. (2018). Reef carbonate productivity during quaternary sea level oscillations. *Geochemistry, Geophysics, Geosystems*, *19*(4), 1148–1164. https://doi.org/10.1002/2017gc007335

Iturralde-Vinent, M., & MacPhee, R. D. (1999). *Paleogeography of the Caribbean region: Implications for Cenozoic biogeography* (p. 238). Bulletin of the AMNH.

Iturralde-Vinent, M. A. (1994). Cuban geology: A new plate-tectonic synthesis. *Journal of Petroleum Geology*, *17*(1), 39–69. https://doi.org/10.1111/j.1747-5457.1994.tb00113.x

Iturralde-Vinent, M. A. (2003). Ensayo sobre la paleogeografía del Cuaternario de Cuba. In *Memorias V Congreso Cubano de Geología y Minería* (p. 74). CD ROM.

Iturralde-Vinent, M. A. (Ed.). (2009). *Geología de Cuba para todos*. Editorial Científico-Técnica.

Jaffey, A. H., Flynn, K. F., Glendenin, L. E., Bentley, W. T., & Essling, A. M. (1971). Precision measurement of half-lives and specific activities of U 235 and U 238. *Physical Review C*, *4*(5), 1889–1906. https://doi.org/10.1103/physrevc.4.1889

Ladd, J. W., & Sheridan, R. E. (1987). Seismic stratigraphy of the Bahamas. *AAPG Bulletin*, *71*(6), 719–736.

Lajoie, K. R. (1986). Coastal tectonics. *Active tectonics*, 95–124.

Leroy, S., de Lépinay, B. M., Mauffret, A., & Pubellier, M. (1996). Structural and tectonic evolution of the eastern Cayman Trough (Caribbean Sea) from seismic reflection data. *AAPG Bulletin*, *80*(2), 222–247.

Leroy, S., Ellouz-Zimmermann, N., Corbeau, J., Rolandone, F., de Lepinay, B. M., Meyer, B., et al. (2015). Segmentation and kinematics of the North America-Caribbean plate boundary offshore Hispaniola. *Terra Nova*, *27*(6), 467–478. https://doi.org/10.1111/ter.12181

Leroy, S., Mauffret, A., Patriat, P., & Mercier de Lépinay, B. (2000). An alternative interpretation of the Cayman trough evolution from a reidentification of magnetic anomalies. *Geophysical Journal International*, *141*(3), 539–557. https://doi.org/10.1046/j.1365-246x.2000.00059.x

Major, J., Harris, R., Chiang, H. W., Cox, N., Shen, C. C., Nelson, S. T., et al. (2013). Quaternary hinterland evolution of the active Banda Arc: Surface uplift and neotectonic deformation recorded by coral terraces at Kisar, Indonesia. *Journal of Asian Earth Sciences*, *73*, 149–161. https://doi.org/10.1016/j.jseaes.2013.04.023

Mann, P. (1997). Model for the formation of large, transtensional basins in zones of tectonic escape. *Geology*, *25*(3), 211–214. https://doi.org/10.1130/0091-7613(1997)025<0211:mftfol>2.3.co;2

Mann, P., Calais, E., & Huerfano, V. (2004). Earthquake shakes "Big Bend" region of North America-Caribbean boundary zone. *Eos, Transactions American Geophysical Union*, *85*(8), 77–83. https://doi.org/10.1029/2004eo080001

Mann, P., Calais, E., Ruegg, J. C., DeMets, C., Jansma, P. E., & Mattioli, G. S. (2002). Oblique collision in the northeastern Caribbean from GPS measurements and geological observations. *Tectonics*, *21*(6), 7–1. https://doi.org/10.1029/2001tc001304

Mann, P., Schubert, C., & Burke, K. (1991). Review of Caribbean neotectonics.

Mann, P., Taylor, F. W., Edwards, R. L., & Ku, T. L. (1995). Actively evolving microplate formation by oblique collision and sideways motion along strike-slip faults: An example from the northeastern Caribbean plate margin. *Tectonophysics*, *246*(1–3), 1–69. https://doi.org/10.1016/0040-1951(94)00268-e

Mauffret, A., & Leroy, S. (1997). Seismic stratigraphy and structure of the Caribbean igneous province. *Tectonophysics*, *283*(1–4), 61–104. https://doi.org/10.1016/s0040-1951(97)00103-0

Mauffret, A., & Leroy, S. (1999). Neogene intraplate deformation of the Caribbean plate at the Beata Ridge. In P. Mann (Ed.), *Sedimentary basins of the world; Caribbean basins* (pp. 627–669). Elsevier Science B.V.

Moreno, B., Grandison, M., & Atakan, K. (2002). Crustal velocity model along the southern Cuban margin: Implications for the tectonic regime at an active plate boundary. *Geophysical Journal International*, *151*(2), 632–645. https://doi.org/10.1046/j.1365-246x.2002.01810.x

Muhs, D. R., Schweig, E. S., Simmons, K. R., & Halley, R. B. (2017). Late Quaternary uplift along the North America-Caribbean plate boundary: Evidence from the sea level record of Guantanamo Bay, Cuba. *Quaternary Science Reviews*, *178*, 54–76. https://doi.org/10.1016/j.quascirev.2017.10.024

Murray-Wallace, C. V., & Woodroffe, C. D. (2014). *Quaternary sea-level changes: A global perspective*. Cambridge University Press.

Mylroie, J. E., & Carew, J. L. (1990). The flank margin model for dissolution cave development in carbonate platforms. *Earth Surface Processes and Landforms*, *15*(5), 413–424. https://doi.org/10.1002/esp.3290150505

Núñez, D., Córdoba, D., & Kissling, E. (2019). Seismic structure of the crust in the western Dominican Republic. *Tectonophysics*, *773*, 228224. https://doi.org/10.1016/j.tecto.2019.228224

Núñez Jiménez, A. (1973). *Geografía de Cuba* (Vol. 4). Editorial Pueblo y Educación.

Oliveira de Sá, A., d'Acremont, E., Leroy, S., & Lafuerza, S. (2021). Polyphase deformation and Strain migration on the septentrional-Oriente Fault Zone in the Windward passage, Northern Caribbean Plate Boundary. *Tectonics*, *40*(8), e2021TC006802. https://doi.org/10.1029/2021tc006802

Pastier, A. M., Husson, L., Pedoja, K., Bézos, A., Authemayou, C., Arias-Ruiz, C., & Cahyarini, S. Y. (2019). Genesis and architecture of sequences of Quaternary coral reef terraces: Insights from numerical models. *Geochemistry, Geophysics, Geosystems*, *20*(8), 4248–4272. https://doi.org/10.1029/2019gc008239

Pedoja, K., Husson, L., Bézos, A., Pastier, A. M., Imran, A. M., Arias-Ruiz, C., et al. (2018). On the long-lasting sequences of coral reef terraces from SE Sulawesi (Indonesia): Distribution, formation, and global significance. *Quaternary Science Reviews*, *188*, 37–57. https://doi.org/10.1016/j.quascirev.2018.03.033

Pedoja, K., Husson, L., Johnson, M. E., Melnick, D., Witt, C., Pochat, S., et al. (2014). Coastal staircase sequences reflecting sea-level oscillations and tectonic uplift during the Quaternary and Neogene. *Earth-Science Reviews*, *132*, 13–38, https://doi.org/10.1016/j.earscirev.2014.01.007

Pedoja, K., Husson, L., Regard, V., Cobbold, P. R., Ostanciaux, E., Johnson, M. E., et al. (2011). Relative sea-level fall since the last interglacial stage: are coasts uplifting worldwide? *Earth-Science Reviews*, *108*(1–2), 1–15. https://doi.org/10.1016/j.earscirev.2011.05.002

Peñalver, L., Pedoja, K., Martin-Izquierdo, D., Authemayou, C., Nuñez, A., Chauveau, D., et al. (2021). The Cuban staircase sequences of coral reef and marine terraces: A forgotten masterpiece of the Caribbean geodynamical puzzle. *Marine Geology*, *440*, 106575. https://doi.org/10.1016/j.margeo.2021.106575

Peñalver, L. L., Castellanos, E., Perez, R., & Rivada, R. (2003). Las terrazas marinas de Cuba y su correlacon con algunas del area circumcaribe. In *Geologia del Cuaternario, geomorfolog˜Aa y carso* (pp. 1–10). La Habana, Memorias Geominerales.

Pindell, J., & Dewey, J. F. (1982). Permo-Triassic reconstruction of western Pangea and the evolution of the Gulf of Mexico/Caribbean region. *Tectonics*, *1*(2), 179–211. https://doi.org/10.1029/tc001i002p00179

Pindell, J., Kennan, L., Maresch, W. V., Stanek, K., Draper, G., & Higgs, R. (2005). Plate-kinematics and crustal dynamics of circum-Caribbean arc-continent interactions: Tectonic controls on basin development in Proto-Caribbean margins. *Special Papers - Geological Society of America*, *394*, 7.

Pons-Branchu, E., Bourrillon, R., Conkey, M. W., Fontugne, M., Fritz, C., Gárate, D., et al. (2014). Uranium-series dating of carbonate formations overlying Paleolithic art: Interest and limitations. *Bulletin de la Societe Prehistorique Française*, *111*(2), 211–224. https://doi.org/10.3406/bspf.2014.14395

Portell, R. W., Klose, W., McCleskey, T., & Toomey, J. K. (2009). *Fossil invertebrates of the U.S. Naval Station Guantanamo Bay, Cuba, Part 2, Pleistocene Corals* (p. 28). Division of Invertebrate Paleontology, Florida Museum of Natural History.

Portell, R. W., McCleskey, T., & Toomey, J. K. (2008). *Fossil invertebrates of the U.S. Naval Station Guantanamo Bay, Cuba, Part 1, Pleistocene Marine mollusca* (p. 32). Division of Invertebrate Paleontology, Florida Museum of Natural History.

Pubellier, M., Mauffret, A., Leroy, S., Vila, M., & Amilcar, H. (2000). Plate boundary readjustment in oblique convergence: Example of the Neogene of Hispaniola, Greater Antilles. *Tectonics*, *19*(4), 630–648. https://doi.org/10.1029/2000tc900007

Rodríguez-Zurrunero, A., Granja-Bruña, J. L., Carbó-Gorosabel, A., Muñoz-Martín, A., Gorosabel-Araus, J. M., de la Peña, L. G., et al. (2019). Submarine morpho-structure and active processes along the North American-Caribbean plate boundary (Dominican Republic sector). *Marine Geology*, *407*, 121–147. https://doi.org/10.1016/j.margeo.2018.10.010

Rodríguez-Zurrunero, A., Granja-Bruña, J. L., Muñoz-Martín, A., Leroy, S., ten Brink, U., Gorosabel-Araus, J. M., et al. (2020). Along-strike segmentation in the northern Caribbean plate boundary zone (Hispaniola sector): Tectonic implications. *Tectonophysics*, *776*, 228322. https://doi.org/10.1016/j.tecto.2020.228322

Rojas-Agramonte, Y., Neubauer, F., Bojar, A. V., Hejl, E., Handler, R., & Delgado, D. E. G. (2006). Geology, age and tectonic evolution of the Sierra Maestra Mountains, southeastern Cuba. *Geológica Acta*, 123.

Román, Y. A., Pujols, E. J., Cavosie, A. J., & Stockli, D. F. (2021). Timing and magnitude of progressive exhumation and deformation associated with Eocene arc-continent collision in the NE Caribbean plate. *GSA Bulletin*, *133*(5–6), 1256–1266. https://doi.org/10.1130/b35715.1

Rosencrantz, E. (1990). Structure and tectonics of the Yucatan Basin, Caribbean Sea, as determined from seismic reflection studies. *Tectonics*, *9*(5), 1037–1059. https://doi.org/10.1029/tc009i005p01037

Rovere, A., Raymo, M. E., Vacchi, M., Lorscheid, T., Stocchi, P., Gomez-Pujol, L., et al. (2016). The analysis of Last Interglacial (MIS 5e) relative sea-level indicators: Reconstructing sea-level in a warmer world. *Earth-Science Reviews*, *159*, 404–427. https://doi.org/10.1016/j.earscirev.2016.06.006

Saura, E., Vergés, J., Brown, D., Lukito, P., Soriano, S., Torrescusa, S., et al. (2008). Structural and tectonic evolution of western Cuba fold and thrust belt. *Tectonics*, *27*(4). https://doi.org/10.1029/2007tc002237

Schielein, P., Burow, C., Pajon, J., Consuegra, R. R., Zhao, J. X., & Schellmann, G. (2020). ESR and U-Th dating results for Last Interglacial coral reef terraces at the northern coast of Cuba. *Quaternary International*, *556*, 216–229. https://doi.org/10.1016/j.quaint.2019.11.041

Stirling, C. H., Esat, T. M., Lambeck, K., & McCulloch, M. T. (1998). Timing and duration of the Last Interglacial: Evidence for a restricted interval of widespread coral reef growth. *Earth and Planetary Science Letters*, *160*(3–4), 745–762. https://doi.org/10.1016/s0012-821x(98)00125-3

Symithe, S., Calais, E., De Chabalier, J. B., Robertson, R., & Higgins, M. (2015). Current block motions and strain accumulation on active faults in the Caribbean. *Journal of Geophysical Research: Solid Earth*, *120*(5), 3748–3774. https://doi.org/10.1002/2014jb011779

Ten Brink, U. (2005). Vertical motions of the Puerto Rico Trench and Puerto Rico and their cause. *Journal of Geophysical Research*, *110*(B6), B06404. https://doi.org/10.1029/2004jb003459

Terence Edgar, N., Ewing, J. I., & Hennion, J. (1971). Seismic refraction and reflection in Caribbean Sea. *AAPG Bulletin*, *55*(6), 833–870.

Toscano, M. A., Rodriguez, E., & Lundberg, J. (1999). Geologic investigation of the late Pleistocene Jaimanitas formation: Science and society in Castro's Cuba.

Uchupi, E., Milliman, J. D., Luyendyk, B. P., Bowin, C. O., & Emery, K. O. (1971). Structure and origin of southeastern Bahamas. *AAPG Bulletin*, *55*(5), 687–704. https://doi.org/10.1306/819A3C56-16C5-11D7-8645000102C1865D

van Benthem, S., Govers, R., & Wortel, R. (2014). What drives microplate motion and deformation in the northeastern Caribbean plate boundary region? *Tectonics*, *33*(5), 850–873. https://doi.org/10.1002/2013tc003402

Vaughan, T. W., & Spencer, A. C. (1902). The geography of Cuba. *Bulletin of the American Geographical Society*, *34*(2), 105–116. https://doi.org/10.2307/197566

Vila, J. M., Jany, I., Lepvrier, C., & Mauffret, A. (1990). Le poinçonnement d'Hispaniola par la ride de Beata (Antilles), données marines et terrestres définissant les trajectoires de contraintes. *Reunion Annuelle des Sciences de la Terre*, *13*.

Weiss, T. L., Linsley, B. K., Gordon, A. L., Rosenthal, Y., & Dannenmann-Di Palma, S. (2022). Constraints on marine isotope stage 3 and 5 sea level from the flooding history of the Karimata Strait in Indonesia. *Paleoceanography and Paleoclimatology*, *37*(9), e2021PA004361. https://doi.org/10.1029/2021pa004361

Wessels, R. J. (2019). Strike-slip fault systems along the northern Caribbean plate boundary. In *Transform plate boundaries and fracture zones* (pp. 375–395). Elsevier.

Yang, F., Sun, W., Hu, Y., & Long, S. (2015). Cationic flotation of scheelite from calcite using quaternary ammonium salts as collector: Adsorption behavior and mechanism. *Minerals Engineering*, *81*, 18–28. https://doi.org/10.1016/j.mineng.2015.07.014